Reflection coefficient of a natural sodium bentonite in aqueous mixed electrolyte solutions: positive and negative anomalous osmosis

Canadian Geotechnical Journal

OPEN ACCESS | Research Article

Reflection coefficient of a natural sodium bentonite in aqueous mixed electrolyte solutions: positive and negative anomalous osmosis

Nicolò Guarena, Andrea Dominijanni, and Mario Manassero

Department of Structural, Geotechnical and Building Engineering, Polytechnic University of Turin, Corso Duca degli Abruzzi 24, 10129 Turin, Italy

Corresponding author: **Nicolò Guarena** (email: nicolo.guarena@polito.it)

Abstract

A natural sodium bentonite was tested in the laboratory to measure its reflection coefficient, ω, in equilibrium with mixed aqueous solutions of sodium chloride (NaCl) and potassium chloride (KCl), with the aim of assessing the relative contribution of chemico-osmosis and diffusion induced electro-osmosis to the non-hydraulic component of the liquid flux in the presence of two cationic species, which diffuse at different rates in the pore solution. The former chemico-osmotic contribution is only related to the ionic partition effect in the bentonite pores, and causes ω to vary in the 0 to 1 range, whereas the latter electro-osmotic contribution is controlled by the diffusion potential, which spontaneously builds up across the bentonite layer in response to the different aqueous-phase diffusion coefficients of the ionic species. The theoretical interpretation of the obtained test results demonstrated that chemico-osmosis was the major contribution to ω when the testing solutions only comprised KCl. However, significant deviations in the values of ω from those expected for pure chemico-osmosis were observed for mixtures of NaCl and KCl, with both negative ($\omega = -1.234$) and positive ($\omega = 1.040$) anomalous values of the reflection coefficient, resulting from the enhanced influence of diffusion induced electro-osmosis.

Key words: chemico-osmosis, diffusion potential, electro-osmosis, geosynthetic clay liners, semipermeable membrane behaviour

Introduction

Smectite-rich clay soils (e.g., bentonites), in addition to having extremely low hydraulic conductivity values (typically $\leq 10^{-11}$ m/s) when permeated with dilute aqueous solutions and self-healing properties due to the high swelling potential, are able to exhibit semipermeable membrane behaviour, which results from the partial restriction of the migration of ionic species through pores that are freely accessible to water (H_2O) molecules. Bentonites have large enough pore sizes to accommodate hydrated ions and the selective restriction of charged solutes cannot therefore be attributed to steric hindrance, which arises when the molecules are larger than the membrane pores, but should instead be attributed to the electrical interactions that occur between the ions in solution and the clay particles (Mitchell and Soga 2005; Shackelford 2013; Shackelford et al. 2019; Manassero 2020), which carry a net negative charge as a consequence of the isomorphic substitution of lower-valence cations for higher-valence cations within the crystal lattice.

Although a conservative assessment of the performance of engineered bentonite-based containment barriers (e.g., geosynthetic clay liners, bentonite-amended soil liners, and soil-bentonite backfills for vertical cutoff walls) can be obtained by modelling pollutant migration according to the classical advective-diffusive transport theory, such barriers are generally able to restrict contaminant migration more effectively as a result of their semipermeable properties, which are responsible, among several coupled transport processes, for the chemico-osmotic phenomenon (Malusis and Shackelford 2002*a*; Manassero and Dominijanni 2003; Malusis et al. 2003, 2012, 2020, 2021; Guarena et al. 2020). Accordingly, extensive research has been conducted over the past few decades to gain a better understanding of the fundamental mechanisms that govern clay membrane behaviour, which is usually quantified through the laboratory measurement of the reflection coefficient, ω, also known as the chemico-osmotic or membrane efficiency coefficient. Most experimental studies have been devoted to investigating the extent to which the reflection coefficient of bentonite-based barriers is affected by the soil porosity and the salt (1:1 type electrolyte) concentration of the equilibrium bulk solutions (Malusis and Shackelford 2002*b*, 2002*c*; Bohnhoff and Shackelford 2013, 2015; Dominijanni et al. 2013, 2018; Malusis and Daniyarov 2016; Shackelford et al. 2016; Musso et al. 2017; Tong and Sample-Lord 2022), the concentration of divalent cations resulting from the dissociation of 2:1 type electrolytes

(Shackelford and Lee 2003; Mazzieri et al. 2010; Bohnhoff et al. 2014; Di Emidio et al. 2015; Fu et al. 2021; Ni et al. 2022), the bentonite content in soil-bentonite mixtures (Yeo et al. 2005; Henning et al. 2006; Evans et al. 2008; Kang and Shackelford 2010; Tang et al. 2014, 2015; Meier and Shackelford 2017), the effective confining stress (Kang and Shackelford 2011; Malusis et al. 2015), and the degree of water saturation (Sample-Lord and Shackelford 2018).

On the basis of the results of the aforementioned studies, the reflection coefficient of bentonite-based barriers is generally considered to vary from zero ($\omega = 0$), in the case of the absence of semipermeable membrane behaviour, to unity ($\omega = 1$), in the case of ideal or perfect clay membranes, which are able to completely prevent anions from entering the pores. However, the range of variation of such phenomenological parameter is not restricted to 0 and 1 on thermodynamic grounds, since ω values outside the 0 to 1 range are fully compatible with the requirement of a non-negative rate of entropy production due to the coupled fluxes of solvent, solutes, and electric current (Dominijanni and Manassero 2012*a*). Furthermore, the soil science and geotechnical engineering literature has provided experimental evidence of the occurrence of the so-called "negative anomalous osmosis", $\omega < 0$, in chemically active clays, whereby the liquid flux is directed against the osmotic pressure gradient under isobaric conditions (Kemper and Quirk 1972; Elrick et al. 1976; Olsen et al. 1989; Keijzer et al. 1999).

Kemper and Quirk (1972) measured the ω parameter of bentonite, illite, and kaolinite clays permeated with aqueous solutions of a single salt, adopting a test configuration that can be classified as an "open hydraulic control system" (Shackelford 2013; Dominijanni et al. 2019*a*). In addition to the osmotic liquid flux, their testing apparatus allowed the electromotive force of the system to be measured through a pair of silver-coated electrodes reversible to Cl^- ions (i.e., Ag/AgCl electrodes) under non-short-circuited conditions, while the known chloride concentration difference allowed the portion of the total electromotive force, due to the electric potential difference established across the specimen, to be estimated. After an initial period in which positive ω values were obtained in equilibrium with dilute solutions, a reversal of the osmotic flow direction occurred for higher salt concentrations, with lower negative ω values generally being detected in the presence of salts that had dissociated into low-mobility multivalent cationic species ($CaCl_2$ and $LaCl_3$). This reversal occurred approximately for the same salt concentration at which the electric potential difference changed sign.

The occurrence of negative anomalous osmosis under isothermal and null-electric-current-density conditions, as in the case of the laboratory tests conducted by Kemper and Quirk (1972), should be attributed to the build-up of an electro-osmotic contribution, which is referred to as diffusion induced electro-osmosis, and causes the measured ω parameter to deviate from the range of variation ($0 \leq \omega \leq 1$) that is expected for pure chemico-osmosis. Indeed, when cations diffuse in the pore solution at a lower rate than anions, a diffusion potential spontaneously develops between the clay boundaries to generate an electromigration of cations in the same direction as that of diffusion and, simultaneously, an electromigration of anions in the opposite direction to that of diffusion. The magnitude of the diffusion potential is such that the resulting fluxes of positive and negative electric charges, as given by the superposition of diffusion and electromigration, are equal to each other, thereby allowing the null-electric-current-density condition to be satisfied. Because of the surplus of a positive electric charge, which is due to the ionic partition effect in the pore solution, electromigration is responsible for a net momentum transfer to the water molecules from the more concentrated solution side to the dilute solution side and, macroscopically, for the build-up of diffusion induced electro-osmosis in the opposite direction to that of chemico-osmosis.

A theoretical investigation of the conditions that are expected to promote such anomalous osmotic behaviour, with emphasis on the role played by diffusion induced electro-osmosis, was conducted by Guarena et al. (2022) in the frame of the uniform-potential approach, which has been widely adopted to model the semipermeable properties of clay soils (e.g., Marine and Fritz 1981; Revil and Leroy 2004; Appelo and Wersin 2007; Jougnot et al. 2009; Dominijanni and Manassero 2012*b*; Manassero et al. 2018). Whenever the pore solution comprises a single cationic species, the osmotically induced water movement through chemically active clays, as driven by a gradient in the ionic concentrations, can be shown to be dominated by chemico-osmosis and any deviation in the measured reflection coefficient from the 0 to 1 range is therefore likely to be modest. This conclusion is consistent with the available experimental evidence concerning negative anomalous osmosis in single-electrolyte and non-short-circuited systems, in which negative ω values lower than – 0.01 have never been reported. However, in the presence of two or more cationic species that have different aqueous-phase diffusion coefficients, the contribution of diffusion induced electro-osmosis to the overall osmotic flow may be comparable to or even greater than that associated with chemico-osmosis, and large deviations in the measured reflection coefficient from the 0 to 1 range are likely to be observed.

Since there is currently no evidence on these latter conditions, and such evidence is of paramount importance to evaluate the field performance of engineered bentonite-based containment barriers, the objective of this paper is to present the results of a multi-stage membrane test carried out on a natural sodium bentonite in contact with aqueous mixtures of sodium chloride and potassium chloride. The obtained results have been interpreted through the theoretical framework outlined by Guarena et al. (2022), with a view to assessing the extent to which the measured reflection coefficient deviates from predictions based on pure chemico-osmosis when two monovalent cations, which diffuse at different rates in water, are simultaneously present in the pore solution. Besides negative anomalous osmosis, the possible occurrence of the so-called "positive anomalous osmosis", $\omega > 1$, as documented by Yaroshchuk et al. (1993) and Hahn and Woermann (1996) for a phenolsulfonic acid-formaldehyde cation exchange membrane, has also been investigated.

Materials and methods

Bentonite and salt solutions

The powdered bentonite tested in this study was the same as the Indian sodium bentonite described by Dominijanni et al. (2013, 2018), which is used for the industrial production of a needle-punched geosynthetic clay liner. The cation exchange capacity was found to vary in the 97 to 104 meq/100 g range by Dominijanni et al. (2019*b*), who adopted the methylene blue titration method as a testing procedure that is able to maintain a dispersed soil fabric and, hence, to enhance the accessibility of the bentonite exchange sites. The mineralogical composition was assessed by Dominijanni et al. (2013) through the X-ray diffraction technique and was observed to mainly consist of smectite (>98%), whereas the other constituents, such as calcite, quartz, mica, and gypsum, were only present in traces. The liquid limit and plastic limit were found to be equal to 525% and 63%, respectively, and the hydraulic conductivity at a 27.5 kPa confining effective stress resulted to be equal to 8×10^{-12} m/s, using deionised water (DW) as the permeant liquid. The specific gravity was equal to 2.65.

The salt solutions were prepared with sodium chloride (NaCl) and potassium chloride (KCl) (ACS reagent, purity $\geq$ 99%, purchased from Merck KGaA, Darmstadt, Germany). Deionised water was used as the solvent (pH = 6.95; $EC_{20°C} = 2$ μS/cm, where $EC_{20°C}$ is the electrical conductivity at a temperature of 20 °C), which was obtained by treating tap water through a series of activated carbon filters, a reverse osmosis process and, finally, an ultraviolet lamp (Elix Water Purification System). The sodium (Na^+) and potassium (K^+) ion concentrations of the liquid samples that were collected during the multi-stage membrane test were measured using inductively coupled plasma optical emission spectrometry or ICP-OES (Optima 2000 DV, produced by Perkin Elmer, Waltham, Mass., USA), whereas the calcium (Ca^{2+}) and magnesium (Mg^{2+}) ion concentrations, which were expected to be significantly lower than the monovalent ion concentrations, were measured using inductively coupled plasma mass spectrometry or ICP-MS (iCAP Q, produced by Thermo Fisher Scientific, Waltham, Mass., USA). As the two double-stage diffusion tests, which were carried out after completion of the multi-stage membrane test to evaluate the matrix tortuosity factor of the porous stones, only involved the use of KCl solutions, the concentration of KCl of the collected liquid samples was determined, in this latter case, from the measured electrical conductivity, EC, according to the calibration curve shown in Fig. 1.

Testing apparatus

The semipermeable properties of the natural sodium bentonite in equilibrium with mixed aqueous solutions of NaCl and KCl were investigated by means of a laboratory apparatus which is similar to that used by Dominijanni et al. (2013) and described in detail by Malusis et al. (2001). The primary components of the testing device are shown in Fig. 2 and include an osmotic cell, a flow-pump accumulator, a differential pressure transducer, and a data acquisition system.

Fig. 1. Calibration of the potassium chloride (KCl) concentration, c_{KCl}, with the measured electrical conductivity, EC. R^2, coefficient of determination for the regression line.

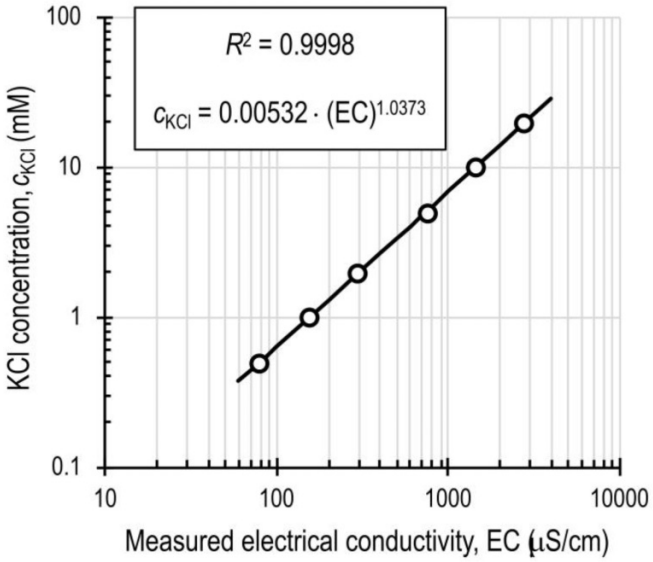

The osmotic cell consists of a modified rigid-wall permeameter (70.57-mm inner diameter), where the top piston and the bottom pedestal are endowed with three drainage lines. The two peripheral lines allow different electrolyte solutions to circulate at the boundaries of the osmotic cell, so that a chemical potential gradient is established across the specimen and is maintained constant throughout the testing stages. The central line is connected to the differential pressure transducer (UNIK 5000 Silicon Pressure Sensor, accuracy ± 0.1% FS BSL, produced by GE Measurement & Control, Billerica, Mass., USA), which enables the difference in hydraulic head, Δh, to be measured between the porous stones. The hydraulic head in the circulation loops through the top piston and the bottom pedestal is monitored by two additional relative pressure transducers. The flow-pump accumulator consists of a dual-carriage syringe pump and two stainless steel actuators (Model 33 Twin Syringe Pump, produced by Harvard, Holliston, Mass., USA), which simultaneously inject and withdraw the same volume of solution from both the upper and lower boundaries of the osmotic cell to prevent a liquid volumetric flux from occurring through the specimen.

Three main differences can be identified between the laboratory apparatus used in this study and the one described by Dominijanni et al. (2013). First, a custom-made steel frame was manufactured and assembled on the osmotic cell to make the top piston stiffer in the vertical direction, so that the void ratio of the specimen was controlled more accurately than in previous studies and, as a result, the condition of null volumetric strain was ensured throughout the test. The fresh salt solutions used to replenish the flow-pump actuators were prepared directly inside two separate filtering flasks, wherein vacuum was applied for a duration of 30 min immediately before each refilling operation to minimise the presence of air in the apparatus. Finally, because of the scattering that was observed by Dominijanni et al. (2013, 2018) in the measured

Fig. 2. Schematic view of the membrane test apparatus (not to scale).

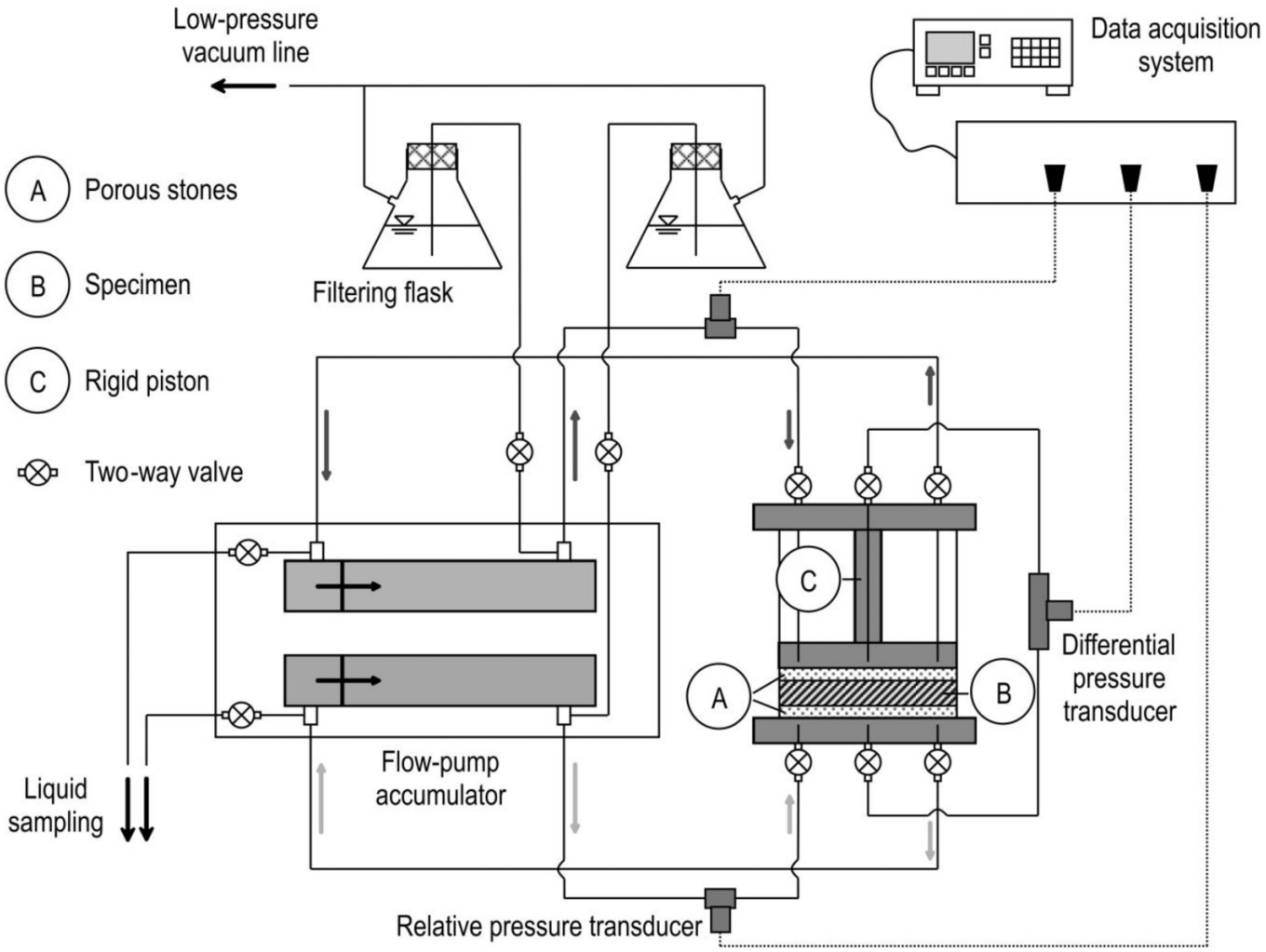

hydraulic head difference, which entailed a certain degree of uncertainty in the determination of the steady-state value of Δh, the osmotic cell was modified by inserting 2-mm-thick brass spacers between the bottom porous stone and the bottom pedestal and, in the same way, between the top porous stone and the top piston, as illustrated in Fig. 3. In this way, the salt solutions were not forced to flow through the porous stones, which had been recognised as the cause of the scattering in the aforementioned experimental measurements, but instead flowed through interstices that were thick enough to avoid any accidental clogging and, hence, exerted negligible resistance to the liquid motion.

Specimen preparation

Prior to membrane testing, the sodium bentonite was subjected to the same "squeezing" procedure that was described in detail by Dominijanni et al. (2013, 2018) to remove any excess soluble salts that are naturally contained in the powdered material. Briefly, this conditioning procedure consists of a series of consecutive phases of hydration with DW and drained consolidation within a consolidometer, while the EC of the sampled solution is periodically measured to evaluate the soluble salt concentration in the bentonite pore water. After approximately six squeezing cycles, the measured EC reached stable values in the 500 to 600 μS/cm range, corresponding to a lower salt concentration than 5 mM. As the EC of the extracted pore water could not be reduced any further simply by advection, the salt removal procedure was terminated at the end of the ninth cycle.

The squeezed sodium bentonite, oven-dried at 105 °C and sifted through an ASTM No. 200 mesh sieve, was hydrated once again with DW up to a water content of 438.5%, which was slightly lower than the liquid limit measured on the raw bentonite. The mixture in the plastic state was then worked with a spatula until a gel-like structure was obtained, which reflects the formation of a dispersed fabric of evenly distributed smectite unit layers (Guyonnet et al. 2005). A known amount of the clay-water mixture (dry mass equal to 21.94 g) was uniformly distributed inside the modified rigid-wall permeameter and sandwiched between two sintered porous stones (28-WF4074, produced by Wykeham Farrance, Liscate, Italy), the physical properties of which are listed in Table 1. Filter papers were placed between the specimen and the porous stones, so as to partially prevent the bentonite particles from migrating into the porous stones. A vertical load was applied to the shaft of the top piston by means

Fig. 3. Detail of the modified rigid-wall permeameter equipped with brass spacers to separate the porous stones from the top piston and the bottom pedestal.

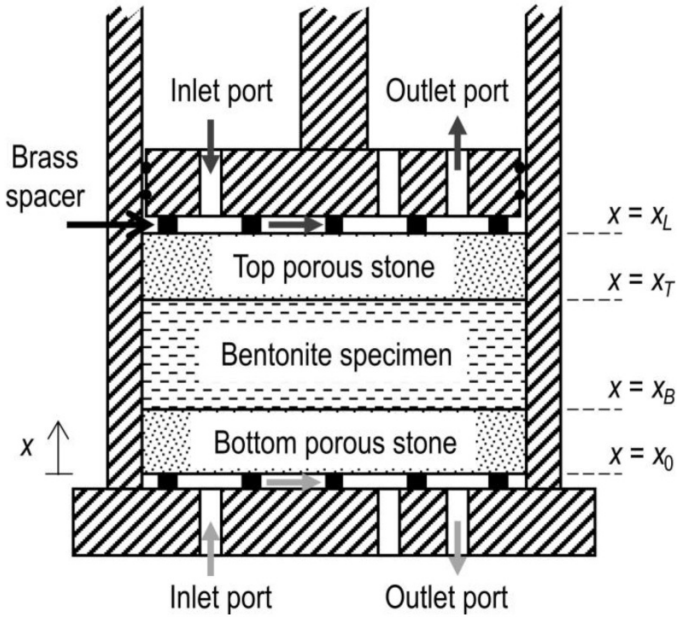

Table 1. Properties of the sintered porous stones (as declared by the manufacturer).

Thickness, L_d (mm)	6
Diameter, d_d (mm)	70
Porosity, n_d (–)	0.43
Hydraulic conductivity, k_d (m/s)	$5 \times 10^{-5} \pm 4 \times 10^{-6}$

of a pneumatic actuator, and gradually increased to consolidate the bentonite specimen under a total vertical stress of 400 kPa. At the end of consolidation, the specimen height, L_b, and its void ratio, e_b, were equal to 10.27 mm and 3.85, respectively. After the piston was locked in place and the drainage lines were connected to the ports of the osmotic cell, DW was continuously infused at both the upper and lower boundaries for a period of 19 days to establish a salt concentration gradient between the pore solution and the external bulk solution, so that the specimen could be further rinsed of any excess soluble salts through a purely diffusive mechanism before membrane testing was initiated. Although the extent of soluble salt removal by this latter purification phase could not be verified, diffusion is expected to be particularly effective when the salt concentrations are so low that purification methods based on advection do not produce any appreciable effect (Sample-Lord and Shackelford 2016).

Testing procedures

The multi-stage membrane test was carried out by circulating different salt solutions through the upper ($x = x_L$) and lower ($x = x_0$) boundaries of the osmotic cell at a circulation rate of 0.05 mL/min, which has been found to be sufficiently fast to minimise the ionic concentration changes that are caused by diffusion through the porous medium and, at the same time, sufficiently slow to allow the ionic molar fluxes to be measured (Malusis et al. 2001, 2015; Dominijanni et al. 2013, 2018). A constant difference in KCl concentration of 9 mM was imposed for the entire duration of the membrane test by maintaining the KCl concentrations of the solutions injected into the upper, $c_{KCl,L}$, and lower, $c_{KCl,0}$, boundaries equal to 10 and 1 mM, respectively. While KCl was the only salt present in the solution circulating through the upper boundary (i.e., $c_{NaCl,L} = 0$), the NaCl concentration of the solution injected into the lower boundary, $c_{NaCl,0}$, was increased stepwise from 0 to 40 mM (Table 2), so that the latter solution corresponded to the hypotonic solution for the first three testing stages and to the hypertonic solution for the last three testing stages.

The hydraulic head difference induced across the specimen and the EC of the solutions exiting from the upper and lower boundaries were measured during all the stages. While Δh was continuously monitored at time increments of 120 s, samples of the solutions exiting from the osmotic cell boundaries were collected for EC measurement when the flow-pump system was briefly halted to refill the hydraulic actuators, which have a capacity of 72 h before the plunger barrel reaches the end of the actuator housing at a circulation rate of 0.05 mL/min. Once steady-state conditions were deemed to have been achieved for each testing stage, on the basis of the measured Δh and EC, the liquid samples collected after the last replenishment of the flow-pump actuators were further analysed to determine the molar concentrations of Na^+, K^+, Ca^{2+}, and Mg^{2+} ions, and the subsequent testing stage was then initiated.

The steady-state molar fluxes of the i-th ionic species entering the upper boundary, $(J_{i,L})_{ss}$, and exiting from the lower boundary, $(J_{i,0})_{ss}$, which were both expected to approach the steady-state molar flux across the specimen, $(J_i)_{ss}$, were determined as follows (Shackelford 1991):

$$(1a) \quad (J_{i,L})_{ss} = \frac{v_w}{A}\left(c_{i,L}^{exit} - c_{i,L}\right)$$

$$(1b) \quad (J_{i,0})_{ss} = \frac{v_w}{A}\left(c_{i,0} - c_{i,0}^{exit}\right)$$

where v_w is the circulation rate imposed by the flow pump (0.05 mL/min), A is the inner cross-sectional area of the rigid-wall permeameter (3.911×10^{-3} m^2), $c_{i,L}$ and $c_{i,0}$ are the concentrations of the i-th ionic species in the solutions injected into the upper and lower boundaries, respectively, $c_{i,L}^{exit}$ and $c_{i,0}^{exit}$ are the steady-state concentrations of the i-th ionic species in the solutions withdrawn from the upper and lower boundaries, respectively.

When the circulation channels in the top piston and bottom pedestal are such that the salt solutions flow outside the porous filter plates, which bind the clay specimen on both sides, and the diffusive resistance of the filter plates themselves is not negligible relative to that of the clay specimen, as is the case with the testing apparatus and natural bentonite used in the present study, it is essential to account for the effect of solute diffusion through the sintered porous stones to correctly assess the transport properties of the tested bentonite (Barbour et al. 1996; Glaus et al. 2008; Yaroshchuk and Van Loon 2008; Yaroshchuk et al. 2008, 2009; Sample-Lord and Shackelford 2018). Therefore, after the apparatus had been disassembled at the end of

Table 2. Measured values of the ionic concentrations and of the hydraulic head difference during the multi-stage membrane test on the natural sodium bentonite.

				Values at steady state								
$c_{NaCl,L}$(mM)	$c_{KCl,L}$(mM)	$c_{NaCl,0}$(mM)	$c_{KCl,0}$(mM)	$c^{exit}_{Na,L}$(mM)	$c^{exit}_{K,L}$(mM)	$c^{exit}_{Ca,L}$(mM)	$c^{exit}_{Mg,L}$(mM)	$c^{exit}_{Na,0}$(mM)	$c^{exit}_{K,0}$(mM)	$c^{exit}_{Ca,0}$(mM)	$c^{exit}_{Mg,0}$(mM)	$(\Delta h)_{ss}$(m)
0	10	0	1	1.45	9.37	0.011	0.022	0.43	0.98	0.001	0.004	1.733
0	10	5	1	1.22	9.28	0.010	0.024	5.23	1.14	0.003	0.010	1.121
0	10	8	1	0.90	9.41	0.009	0.023	8.33	1.23	0.002	0.008	0.510
0	10	12	1	0.80	9.40	0.009	0.022	12.10	1.32	0.003	0.009	0.306
0	10	20	1	0.60	9.89	0.008	0.021	19.62	1.53	0.005	0.015	− 0.204
0	10	40	1	1.09 [a]	10.69 [a]	0.007	0.020	45.59 [a]	1.67 [a]	0.004	0.016	− 0.510

Note: $c_{NaCl,L}$ and $c_{NaCl,0}$, NaCl concentrations of the solutions injected into the upper and lower boundaries, respectively; $c_{KCl,L}$ and $c_{KCl,0}$, KCl concentrations of the solutions injected into the upper and lower boundaries, respectively; $c^{exit}_{i,L}$ and $c^{exit}_{i,0}$, concentrations of the *i*-th ionic species of the solutions withdrawn from the upper and lower boundaries, respectively; $(\Delta h)_{ss}$, difference in hydraulic head of the bulk solution across the specimen.
[a] The marked values of ionic concentration were not used to calculate the ionic molar fluxes.

Table 3. Measured values of the KCl concentration during the double-stage diffusion tests on the porous stones.

					Values at steady state			
	$c_{NaCl,L}$(mM)	$c_{KCl,L}$(mM)	$c_{NaCl,0}$(mM)	$c_{KCl,0}$(mM)	$c^{exit}_{KCl,L}$(mM)	$c^{exit}_{KCl,0}$(mM)	$c^{avg}_{KCl,L}$(mM)	$c^{avg}_{KCl,0}$(mM)
Top porous stone	0	10	0	0	9.30	0.83	9.65	0.41
	0	20	0	0	17.89	1.78	18.94	0.89
Bottom porous stone	0	10	0	0	9.34	0.73	9.67	0.36
	0	20	0	0	18.48	1.61	19.24	0.81

Note: $c_{NaCl,L}$ and $c_{NaCl,0}$, NaCl concentrations of the solutions injected into the upper and lower boundaries, respectively; $c_{KCl,L}$ and $c_{KCl,0}$, KCl concentrations of the solutions injected into the upper and lower boundaries, respectively; $c^{exit}_{KCl,L}$ and $c^{exit}_{KCl,0}$, KCl concentrations of the solutions withdrawn from the upper and lower boundaries, respectively; $c^{avg}_{KCl,L}$ and $c^{avg}_{KCl,0}$, average KCl concentrations of the solutions circulating at the upper and lower boundaries, respectively.

the membrane test, any bentonite adhering to the surface of the porous stones was mechanically removed and the porous stones were allowed to equilibrate with DW. Two double-stage diffusion tests were then conducted to measure the diffusive properties of the porous stones in the "used" state, i.e., after an overall contact time of 131 days with the bentonite specimen. Each diffusion test was carried out on a single porous stone, using the same modified rigid-wall permeameter and testing procedures that were adopted for membrane testing, but circulating DW at the lower boundary and varying the KCl concentration of the solutions infused at the upper boundary from 10 to 20 mM (Table 3). The porous stones were supported laterally with polytetrafluoroethylene (PTFE) flat seals to prevent sidewall diffusion from occurring, and care was taken to avoid any difference in hydraulic head between the upper and lower boundaries during the refilling phases of the flow-pump actuators.

Since any residual soluble salts were removed from the porous stones through equilibration with DW prior to diffusion testing, only K^+ and Cl^- ions were assumed to contribute to the measured EC of the sampled solutions, so that the molar concentrations of KCl for the fluxes withdrawn from the upper, $c^{exit}_{KCl,L}$, and lower boundary, $c^{exit}_{KCl,0}$, were estimated from the EC measurements and the calibration curve shown in Fig. 1. Therefore, as opposed to the membrane test, it was possible not only to calculate the steady-state values at each testing stage but also the trends over time of the KCl molar fluxes entering the upper boundary, $J_{KCl,L}$, and exiting from the lower boundary, $J_{KCl,0}$, as follows:

$$(2a)\quad J_{KCl,L} = \frac{v_w}{A}\left(c^{exit}_{KCl,L} - c_{KCl,L}\right)$$

$$(2b)\quad J_{KCl,0} = \frac{v_w}{A}\left(c_{KCl,0} - c^{exit}_{KCl,0}\right)$$

Under steady-state conditions, the trends over time of the $J_{KCl,L}$ and $J_{KCl,0}$ fluxes were expected to approach the same asymptotic value, corresponding to the steady-state molar flux, $(J_{KCl})_{ss}$.

Test results

The multi-stage membrane test was performed using squeezed sodium bentonite, which had preliminarily been hydrated with DW up to a water content that was close to the liquid limit, then worked with a spatula to promote the formation of a dispersed fabric and, finally, consolidated until a height of 10.27 mm was attained (i.e., $e_b = 3.85$). The a priori estimated e_b was verified at the end of the test by measuring the water content of the bentonite, which resulted to be equal to 145.3%.

The measured difference in hydraulic head between the upper and lower boundaries of the osmotic cell is shown in Fig. 4 as a function of time. The estimation of the steady-state values of the hydraulic head difference, $(\Delta h)_{ss}$, which are reported in Table 2, was based on a critical examination of the overall experimental trend, and steady-state conditions were found to be achieved after approximately two weeks from the beginning of each testing stage. Therefore, apart from the first two stages, which were prolonged for a period of 21 days, each of the remaining stages lasted 14 days.

Similar conclusions can be drawn from an analysis of the trend over time of the measured increase in electrical conductivity of the solution circulating through the upper boundary, ΔEC_L, and the decrease in electrical conductivity of the solution circulating through the lower boundary, ΔEC_0:

$$(3a)\quad \Delta EC_L = EC^{exit}_L - EC_L$$

Fig. 4. Hydraulic head difference, Δh, as a function of time during the multi-stage membrane test conducted on the natural sodium bentonite.

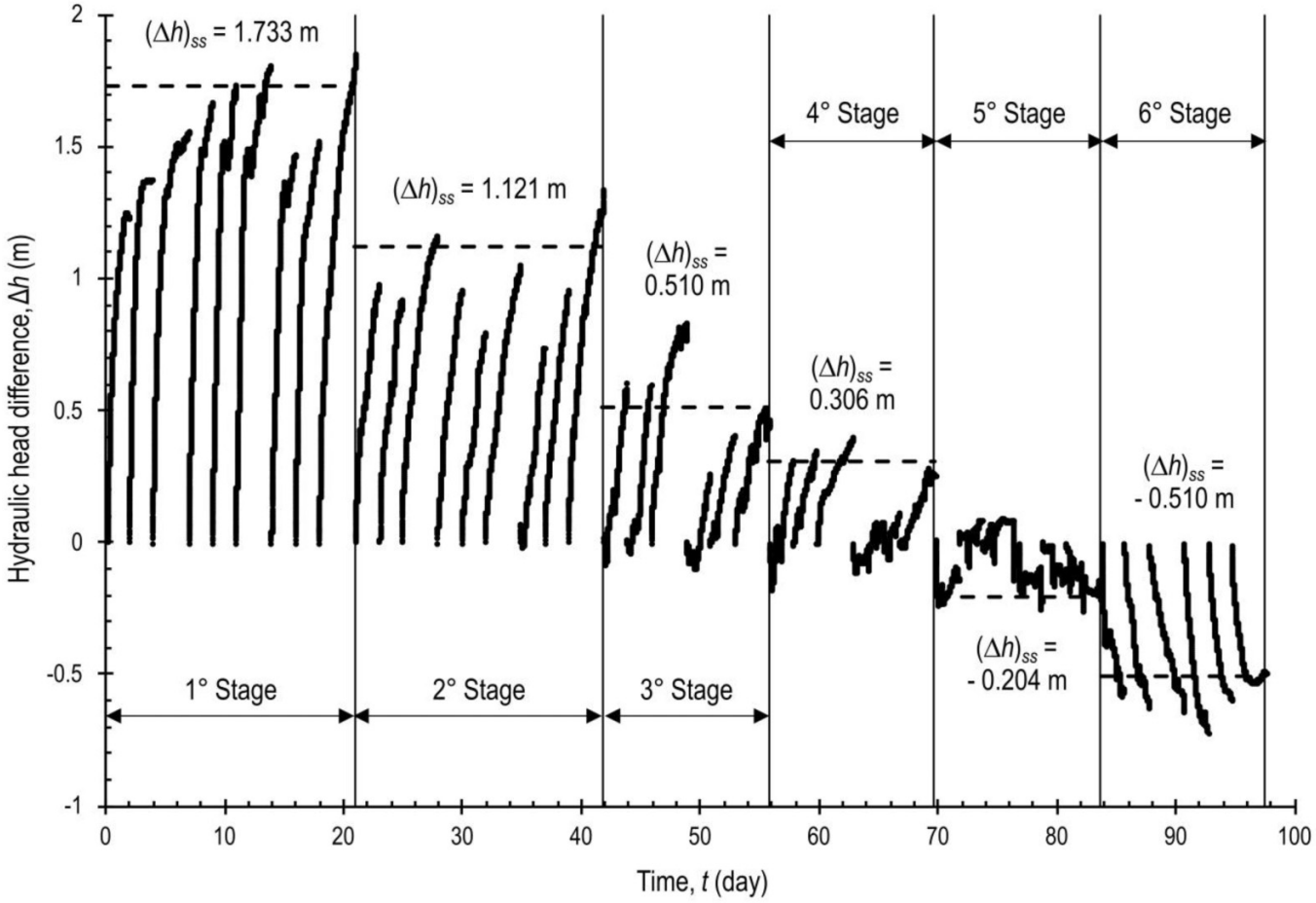

(3b) $$\Delta EC_0 = EC_0 - EC_0^{exit}$$

where EC_L and EC_0 are the electrical conductivities of the salt solutions injected into the upper and lower boundaries, respectively, EC_L^{exit} and EC_0^{exit} are the electrical conductivities of the salt solutions withdrawn from the upper and lower boundaries, respectively.

Although both ΔEC_L and ΔEC_0 approached steady-state values after a period of approximately two weeks from the beginning of each testing stage, ΔEC_L eventually overcame ΔEC_0 in all the stages (Fig. 5). As discussed by Dominijanni et al. (2018), the observed phenomenon can be ascribed to the presence of excess soluble salts in the bentonite pores that had not been entirely removed by the implemented purification procedures and, hence, contributed to a certain extent to the EC measurements during membrane testing.

The above evidence was confirmed from the measured concentrations of the ionic species in the circulation outflows (Table 2) and the ionic molar fluxes that were calculated according to eqs. 1a and 1b (Table 4). Indeed, although the Ca^{2+} and Mg^{2+} concentrations were negligible for all the testing stages and, thus, were assumed to be null for the theoretical interpretation of the obtained test results, $(J_{i,L})_{ss}$ and $(J_{i,0})_{ss}$ were found to diverge from each other due to the presence of residual soluble NaCl in the pore solution. In particular, $(J_{Na,L})_{ss}$ was larger than $(J_{Na,0})_{ss}$, thereby suggesting an outward migration of soluble Na^+ ions from the bentonite specimen to both the upper and lower boundaries of the osmotic cell. Such outward migration of soluble Na^+ ions was found to be compensated by an inward migration of K^+ ions from the boundaries of the osmotic cell to the bentonite specimen, since $(J_{K,L})_{ss}$ was lower than $(J_{K,0})_{ss}$. The observed divergence was particularly notable during the early stages, because of the relatively low values of the boundary salt concentrations, thus the steady-state molar fluxes of Na^+ and K^+ ions across the specimen were assessed by averaging $(J_{i,L})_{ss}$ and $(J_{i,0})_{ss}$ to reduce the error that had been introduced by this contribution (Table 4):

(4) $$(J_i)_{ss} = \frac{(J_{i,L})_{ss} + (J_{i,0})_{ss}}{2}$$

All the Na^+ and K^+ concentration measurements were used to calculate the fluxes, apart from the concentration values that were measured for the last testing stage. The outcomes of the chemical analyses that were conducted on the liquid samples collected at the end of the sixth stage were not consistent with the imposed boundary salt concentrations and, in general, with the ionic concentrations that had been measured in the earlier stages, thus suggesting that an experimental error might have altered the results of the aforementioned

Fig. 5. Variations in electrical conductivity, ΔEC, of the solutions circulating through the upper and lower boundaries of the osmotic cell as a function of time during the multi-stage membrane test conducted on the natural sodium bentonite.

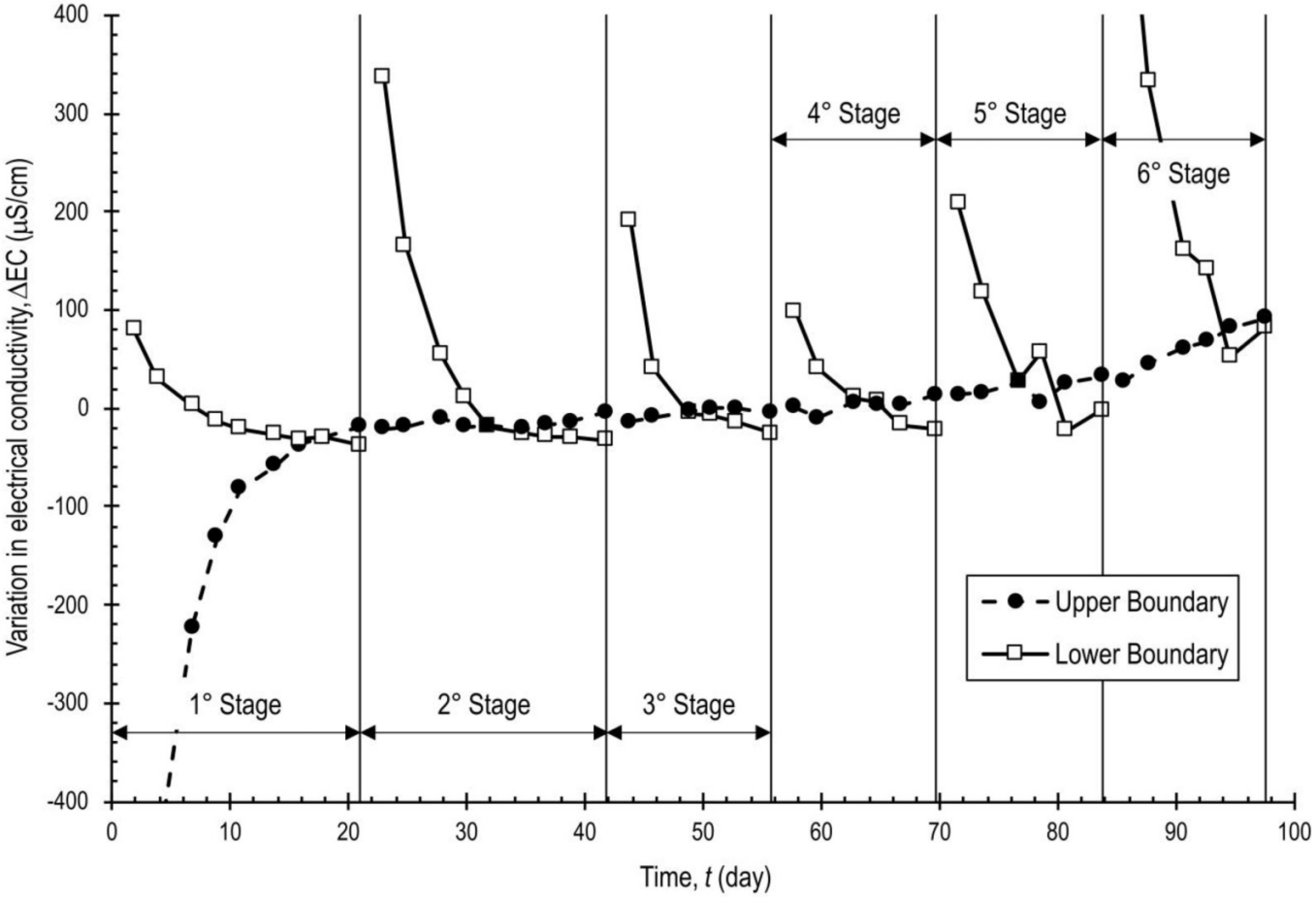

Table 4. Calculated steady-state values of the ionic molar fluxes for the multi-stage membrane test conducted on the natural sodium bentonite (first to fifth testing stages).

$(J_{Na,L})_{ss}$ ($\times 10^{-7}$ mol·m^{-2}·s^{-1})	$(J_{K,L})_{ss}$ ($\times 10^{-7}$ mol·m^{-2}·s^{-1})	$(J_{Na,0})_{ss}$ ($\times 10^{-7}$ mol·m^{-2}·s^{-1})	$(J_{K,0})_{ss}$ ($\times 10^{-7}$ mol·m^{-2}·s^{-1})	$(J_{Na})_{ss}$ ($\times 10^{-7}$ mol·m^{-2}·s^{-1})	$(J_{K})_{ss}$ ($\times 10^{-7}$ mol·m^{-2}·s^{-1})
3.086	−1.350	− 0.908	0.044	1.089	−0.653
2.604	−1.530	− 0.496	− 0.300	1.054	−0.915
1.918	−1.247	− 0.712	− 0.496	0.603	−0.871
1.714	−1.269	− 0.206	− 0.681	0.754	−0.975
1.279	−0.244	0.806	− 1.134	1.042	−0.689

Note: $(J_{i,L})_{ss}$ and $(J_{i,0})_{ss}$, steady-state molar fluxes of the *i*-th ionic species entering the upper boundary and exiting from the lower boundary, respectively; $(J_i)_{ss}$, steady-state molar flux of the *i*-th ionic species across the specimen.

analyses. For this reason, the ionic molar fluxes were not calculated for the sixth testing stage.

The trends of the KCl molar fluxes over time during the two double-stage diffusion tests, which were conducted to assess the diffusive properties of the porous stones, were obtained according to eqs. 2a and 2b, on the basis of the measured KCl concentrations in the circulation outflows (Table 3). Both the first and second stages of the test carried out on the top porous stone lasted 12 days, whereas the first and second stages of the test carried out on the bottom porous stone lasted 14 and 11 days, respectively. As shown in Fig. 6, steady-state conditions were achieved at the end of each testing stage, since $J_{KCl,L}$ and $J_{KCl,0}$ clearly approached the same asymptotic value, which corresponded to $(J_{KCl})_{ss}$ and was determined as follows (Table 5):

$$(5) \qquad (J_{KCl})_{ss} = \frac{(J_{KCl,L})_{ss} + (J_{KCl,0})_{ss}}{2}$$

where $(J_{KCl,L})_{ss}$ and $(J_{KCl,0})_{ss}$ were assumed to coincide with the last calculated values of $J_{KCl,L}$ and $J_{KCl,0}$, respectively, for the considered testing stage.

Fig. 6. Trends of the KCl molar fluxes, J_{KCl}, over time during the double-stage diffusion tests conducted on the porous stones: (*a*) first stage on the top porous stone; (*b*) second stage on the top porous stone; (*c*) first stage on the bottom porous stone; (*d*) second stage on the bottom porous stone.

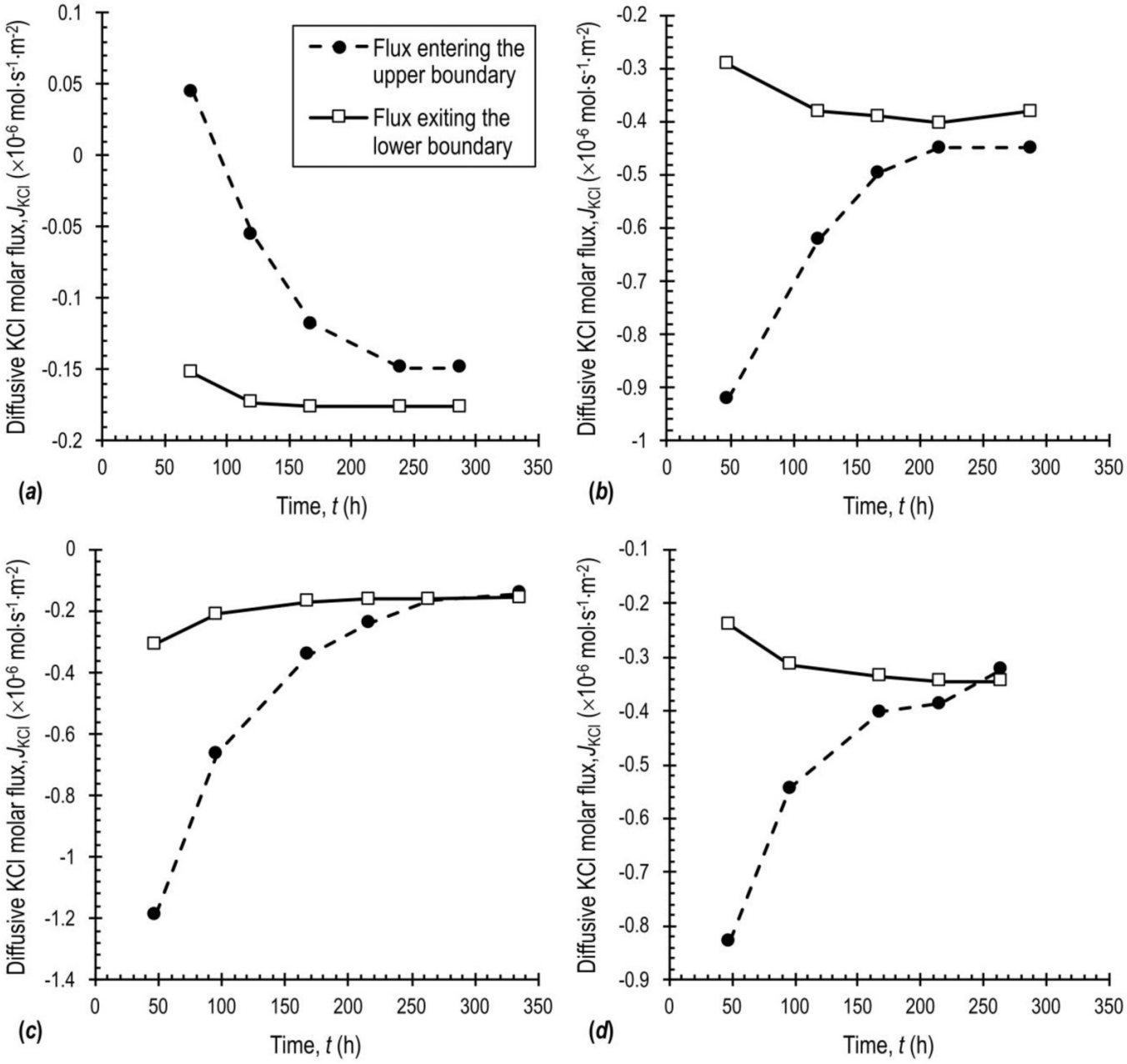

Table 5. Calculated steady-state values of the KCl molar fluxes for the double-stage diffusion tests conducted on the porous stones.

	$(J_{KCl,L})_{ss}$ ($\times 10^{-6}$ mol·m^{-2}·s^{-1})	$(J_{KCl,0})_{ss}$ ($\times 10^{-6}$ mol·m^{-2}·s^{-1})	$(J_{KCl})_{ss}$ ($\times 10^{-6}$ mol·m^{-2}·s^{-1})
Top porous stone	−0.149	−0.176	−0.163
	−0.450	−0.380	−0.415
Bottom porous stone	−0.141	−0.155	−0.148
	−0.324	−0.344	−0.334

Note: $(J_{KCl,L})_{ss}$ and $(J_{KCl,0})_{ss}$, steady-state KCl molar fluxes entering the upper boundary and exiting from the lower boundary, respectively; $(J_{KCl})_{ss}$, steady-state KCl molar flux across the porous stone.

Fig. 7. Linear regression of the steady-state values of the normalised KCl molar flux (open symbols) versus the imposed KCl concentration difference, Δc_{KCl}: (*a*) double-stage diffusion test on the top porous stone; (*b*) double-stage diffusion test on the bottom porous stone. $(J_{KCl})_{ss}$, steady-state KCl molar flux across the porous stone; L_d, thickness of the porous stone; n_d, porosity of the porous stone; and $D_{0,KCl}$, free-solution diffusion coefficient of KCl.

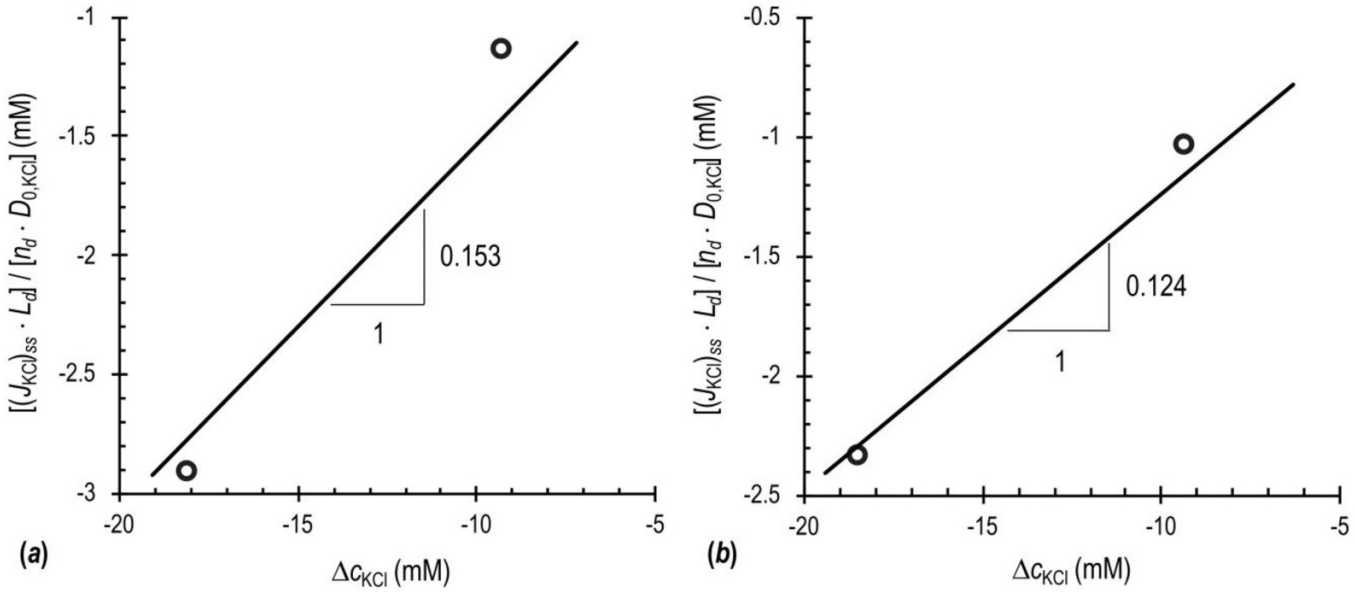

Discussion

Interpretation of double-stage diffusion test results

Since solutions of a single salt (i.e., KCl) were infused at the upper boundary of the rigid-wall permeameter to test the porous stones for their diffusive properties, the following relation holds between the matrix tortuosity factor, $\tau_{m,d}$, of the porous stones, which behave as non-semipermeable porous media, and $(J_{KCl})_{ss}$ under null-volumetric-liquid-flux conditions (Shackelford and Daniel 1991; Manassero and Shackelford 1994):

$$\tau_{m,d} = \frac{L_d}{n_d D_{0,KCl}} \left[\frac{(J_{KCl})_{ss}}{\Delta c_{KCl}} \right]_{q=0} \quad (6)$$

where n_d is the porosity and L_d is the thickness of the porous stones, $D_{0,KCl}$ is the free-solution or aqueous-phase diffusion coefficient of KCl (1.99×10^{-9} m^2/s), and $\Delta c_{KCl} = c^{avg}_{KCl,0} - c^{avg}_{KCl,L}$ is the difference between the average steady-state KCl concentrations at the lower, $c^{avg}_{KCl,0}$, and upper boundary, $c^{avg}_{KCl,L}$, which are defined as follows (Table 3):

$$c^{avg}_{KCl,0} = \frac{c_{KCl,0} + c^{exit}_{KCl,0}}{2} \quad (7a)$$

$$c^{avg}_{KCl,L} = \frac{c_{KCl,L} + c^{exit}_{KCl,L}}{2} \quad (7b)$$

The $\tau_{m,d}$ parameter was independently estimated for the tested porous stones by fitting the experimental data to the linear relation given by eq. 6, wherein $\tau_{m,d}$ represents the slope of the normalised steady-state molar flux of KCl versus Δc_{KCl} (Fig. 7). The matrix tortuosity factor resulted to be equal to 0.153 and 0.124 for the top and bottom porous stones, respectively. Thus, $\tau_{m,d} = 0.139$ was assumed for the theoretical interpretation of the membrane test results as an average value that was representative of both the tested porous stones, since the differences in the measured diffusive properties were within the experimental uncertainty associated with the testing methods.

The estimated value of $\tau_{m,d}$ pertains to the "used" state, in which the diffusive resistance of the porous stones is affected by the bentonite particles that infiltrated during membrane testing, thus leading to changes in the geometry of the diffusive pathways. As such, $\tau_{m,d}$ progressively changed while testing the bentonite specimen for its semipermeable properties and it was therefore not constant over time, *stricto sensu*. However, on the basis of the experimental evidence obtained by Glaus et al. (2008), most of the clogging was expected to have occurred within the first 33 days of contact between the specimen and the porous stones, during which the squeezed sodium bentonite was consolidated and then equilibrated with DW, thus allowing $\tau_{m,d}$ to be regarded as a constant parameter throughout the 98-day-long period of membrane testing.

Interpretation of multi-stage membrane test results

The laboratory apparatus used in the present study can be classified as a "closed hydraulic control system" (Shackelford 2013; Dominijanni et al. 2018, 2019*a*), whereby the magnitude of the hydraulic head difference that is measured across the semipermeable porous medium is such as to counteract the tendency of the osmotic liquid flux, which in turn is induced by an imposed osmotic pressure difference. Under

these testing conditions, the global value of the reflection coefficient at steady state, ω_g, is given by:

$$\omega_g = \left[\frac{\gamma_w (\Delta h)_{ss}}{\Delta \Pi}\right]_{q=0;I=0} \tag{8}$$

where γ_w is the water unit weight (9.81 kN/m^3), $\Delta\Pi$ is the difference in osmotic pressure of the external bulk solution between the top and bottom boundaries of the bentonite specimen, q is the volumetric liquid flux through the bentonite specimen, and I is the electric current density.

$\Delta\Pi$ can be approximated for dilute aqueous solutions by means of the van't Hoff (1887) expression:

$$\Delta \Pi = 2RT\,(c_{\mathrm{Na},T} + c_{\mathrm{K},T} - c_{\mathrm{Na},B} - c_{\mathrm{K},B}) \tag{9}$$

where R is the universal gas constant (8.314 J/mol·K), T is the absolute temperature (293.15 K in the present study), $c_{\mathrm{Na},T}$ and $c_{\mathrm{Na},B}$ are the concentrations of Na^+ ions in the bulk solution at the top and bottom specimen boundaries, respectively, $c_{\mathrm{K},T}$ and $c_{\mathrm{K},B}$ are the concentrations of K^+ ions in the bulk solution at the top and bottom specimen boundaries, respectively.

A physical interpretation of the reflection coefficient of clays in aqueous mixed electrolyte solutions was proposed by Guarena et al. (2022), who resorted to the uniform-potential approach to derive closed-form analytical solutions to the nonlinear differential system that describes the steady-state transport of charged solutes by diffusion and electromigration. Two different mechanisms contribute to determining the macroscopically measured ω_g under null-volumetric-liquid-flux ($q = 0$) and null-electric-current-density ($I = 0$) conditions:

$$\omega_g = \Omega_c + \Omega_e \tag{10}$$

where Ω_c is the chemico-osmotic contribution, which is only related to the ionic partition effect in the pore solution, and Ω_e is the electro-osmotic contribution, which is controlled by the diffusion potential and, thus, is referred to as diffusion induced electro-osmosis.

The chemico-osmotic contribution to the measured reflection coefficient can be assessed as follows:

$$\Omega_c = 1 - \frac{\Delta\overline{\Pi}}{\Delta\Pi} \tag{11}$$

where $\Delta\overline{\Pi}$ is the difference in osmotic pressure of the pore solution between the top and bottom boundaries of the bentonite specimen.

In a similar way to eq. 9, $\Delta\overline{\Pi}$ can be approximated by the van't Hoff (1887) expression:

$$\Delta\overline{\Pi} = RT\,(\bar{c}_{\mathrm{Na},T} + \bar{c}_{\mathrm{K},T} + \bar{c}_{\mathrm{Cl},T} - \bar{c}_{\mathrm{Na},B} - \bar{c}_{\mathrm{K},B} - \bar{c}_{\mathrm{Cl},B}) \tag{12}$$

where $\bar{c}_{\mathrm{Na},T}$ and $\bar{c}_{\mathrm{Na},B}$ are the concentrations of Na^+ ions in the pore solution at the top and bottom specimen boundaries, respectively, $\bar{c}_{\mathrm{K},T}$ and $\bar{c}_{\mathrm{K},B}$ are the concentrations of K^+ ions in the pore solution at the top and bottom specimen boundaries, respectively, $\bar{c}_{\mathrm{Cl},T}$ and $\bar{c}_{\mathrm{Cl},B}$ are the concentrations of Cl^- ions in the pore solution at the top and bottom specimen boundaries, respectively.

The partition coefficients of Cl^- ions at the top, $\Gamma_{\mathrm{Cl},T}$, and bottom, $\Gamma_{\mathrm{Cl},B}$, boundaries of the bentonite specimen are obtained from the statement of macroscopic electroneutrality in the pore solution:

$$\Gamma_{\mathrm{Cl},T} = -\frac{\bar{c}'_{sk,0}}{2e_b\,(c_{\mathrm{Na},T} + c_{\mathrm{K},T})} + \sqrt{\left[\frac{\bar{c}'_{sk,0}}{2e_b\,(c_{\mathrm{Na},T} + c_{\mathrm{K},T})}\right]^2 + 1} \tag{13a}$$

$$\Gamma_{\mathrm{Cl},B} = -\frac{\bar{c}'_{sk,0}}{2e_b\,(c_{\mathrm{Na},B} + c_{\mathrm{K},B})} + \sqrt{\left[\frac{\bar{c}'_{sk,0}}{2e_b\,(c_{\mathrm{Na},B} + c_{\mathrm{K},B})}\right]^2 + 1} \tag{13b}$$

so that the ionic concentrations in the pore solution at the top and bottom specimen boundaries are given by:

$$\bar{c}_{\mathrm{Cl},T} = \Gamma_{\mathrm{Cl},T} \cdot (c_{\mathrm{Na},T} + c_{\mathrm{K},T}) \tag{14a}$$

$$\bar{c}_{\mathrm{Na},T} = (\Gamma_{\mathrm{Cl},T})^{-1} \cdot c_{\mathrm{Na},T} \tag{14b}$$

$$\bar{c}_{\mathrm{K},T} = \frac{\bar{c}'_{sk,0}}{e_b} + \bar{c}_{\mathrm{Cl},T} - \bar{c}_{\mathrm{Na},T} \tag{14c}$$

$$\bar{c}_{\mathrm{Cl},B} = \Gamma_{\mathrm{Cl},B} \cdot (c_{\mathrm{Na},B} + c_{\mathrm{K},B}) \tag{14d}$$

$$\bar{c}_{\mathrm{Na},B} = (\Gamma_{\mathrm{Cl},B})^{-1} \cdot c_{\mathrm{Na},B} \tag{14e}$$

$$\bar{c}_{\mathrm{K},B} = \frac{\bar{c}'_{sk,0}}{e_b} + \bar{c}_{\mathrm{Cl},B} - \bar{c}_{\mathrm{Na},B} \tag{14f}$$

where $\bar{c}'_{sk,0}$ is the solid charge coefficient, which depends on both the bentonite fabric and the cation exchange capacity (Dominijanni et al. 2018, 2019*b*).

The electro-osmotic contribution to the measured reflection coefficient can be assessed as follows:

$$\Omega_e = -F\frac{\bar{c}'_{sk,0}}{e_b}\frac{\Delta\bar{\varphi}_b}{\Delta\Pi} \tag{15}$$

where F is Faraday's constant (9.6485 × 10^4 C/mol) and $\Delta\bar{\varphi}_b$ is the difference in electric potential of the pore solution between the top and bottom boundaries of the bentonite specimen, which corresponds to the diffusion potential and arises to enforce the condition of null electric current density when the ionic species diffuse at different rates in the pore solution.

An approximate analytical solution to the problem of calculating $\Delta\bar{\varphi}_b$ can be obtained on the basis of the constant-field assumption, i.e., on the assumption that the electric potential of the pore solution varies linearly over the length of the porous medium (Goldman 1943). For the considered multi-stage membrane test, which was carried out using solutions of two 1:1 type electrolytes with a common anion, the constant-field assumption leads to the following explicit solution for $\Delta\bar{\varphi}_b$:

$$\Delta\bar{\varphi}_b = \frac{RT}{F} \cdot \ln\left(\frac{D_{0,\mathrm{Na}}\bar{c}_{\mathrm{Na},B} + D_{0,\mathrm{K}}\bar{c}_{\mathrm{K},B} + D_{0,\mathrm{Cl}}\bar{c}_{\mathrm{Cl},T}}{D_{0,\mathrm{Na}}\bar{c}_{\mathrm{Na},T} + D_{0,\mathrm{K}}\bar{c}_{\mathrm{K},T} + D_{0,\mathrm{Cl}}\bar{c}_{\mathrm{Cl},B}}\right) \tag{16}$$

where the free-solution or aqueous-phase diffusion coefficients of sodium, $D_{0,\mathrm{Na}}$, potassium, $D_{0,\mathrm{K}}$, and chloride, $D_{0,\mathrm{Cl}}$, ions at the testing temperature are equal to 1.33 × 10^{-9}, 1.96 × 10^{-9}, and 2.03 × 10^{-9} m^2/s, respectively (Shackelford and Daniel 1991).

The ionic concentrations in the bulk solution at the top and bottom specimen boundaries are not known a priori and, hence, their values need to be determined from the condition

of continuity in the molar fluxes of Na^+ and K^+ ions at steady state. For the adopted testing apparatus, where the bentonite specimen was interposed between two porous stones that exhibited non-negligible resistance to ionic diffusion (Fig. 3), the continuity condition results in the following nonlinear algebraic system of four equations in four unknowns (i.e., $c_{Na,T}$, $c_{K,T}$, $c_{Na,B}$, and $c_{K,B}$):

$$(17a)\quad (J_{Na,b})_{ss} = (J_{Na,dT})_{ss}$$

$$(17b)\quad (J_{K,b})_{ss} = (J_{K,dT})_{ss}$$

$$(17c)\quad (J_{Na,b})_{ss} = (J_{Na,dB})_{ss}$$

$$(17d)\quad (J_{K,b})_{ss} = (J_{K,dB})_{ss}$$

where $(J_{Na,b})_{ss}$, $(J_{Na,dT})_{ss}$, and $(J_{Na,dB})_{ss}$ are the steady-state molar fluxes of Na^+ ions through the bentonite specimen, the top porous stone, and the bottom porous stone, respectively, $(J_{K,b})_{ss}$, $(J_{K,dT})_{ss}$, and $(J_{K,dB})_{ss}$ are the steady-state molar fluxes of K^+ ions through the bentonite specimen, the top porous stone, and the bottom porous stone, respectively.

In the frame of the constant-field theory, the steady-state molar fluxes of Na^+ and K^+ ions through the bentonite specimen can be calculated as follows:

$$(18a)\quad (J_{Na,b})_{ss} = -\frac{n_b \tau_{m,b} D_{0,Na}}{L_b} \frac{F}{RT} \Delta\bar{\varphi}_b \frac{\bar{c}_{Na,T} \exp\left(\frac{F}{RT}\Delta\bar{\varphi}_b\right) - \bar{c}_{Na,B}}{\exp\left(\frac{F}{RT}\Delta\bar{\varphi}_b\right) - 1}$$

$$(18b)\quad (J_{K,b})_{ss} = -\frac{n_b \tau_{m,b} D_{0,K}}{L_b} \frac{F}{RT} \Delta\bar{\varphi}_b \frac{\bar{c}_{K,T} \exp\left(\frac{F}{RT}\Delta\bar{\varphi}_b\right) - \bar{c}_{K,B}}{\exp\left(\frac{F}{RT}\Delta\bar{\varphi}_b\right) - 1}$$

where n_b is the porosity and $\tau_{m,b}$ is the matrix tortuosity factor of the bentonite specimen.

The top and bottom porous stones do not exhibit semipermeable properties, therefore the corresponding steady-state molar fluxes of Na^+ and K^+ ions can be calculated as follows:

$$(19a)\quad (J_{Na,dT})_{ss} = -\frac{n_d \tau_{m,d} D_{0,Na}}{L_d} \frac{F}{RT} \Delta\varphi_{dT} \frac{c_{Na,L} \exp\left(\frac{F}{RT}\Delta\varphi_{dT}\right) - c_{Na,T}}{\exp\left(\frac{F}{RT}\Delta\varphi_{dT}\right) - 1}$$

$$(19b)\quad (J_{K,dT})_{ss} = -\frac{n_d \tau_{m,d} D_{0,K}}{L_d} \frac{F}{RT} \Delta\varphi_{dT} \frac{c_{K,L} \exp\left(\frac{F}{RT}\Delta\varphi_{dT}\right) - c_{K,T}}{\exp\left(\frac{F}{RT}\Delta\varphi_{dT}\right) - 1}$$

$$(19c)\quad (J_{Na,dB})_{ss} = -\frac{n_d \tau_{m,d} D_{0,Na}}{L_d} \frac{F}{RT} \Delta\varphi_{dB} \frac{c_{Na,B} \exp\left(\frac{F}{RT}\Delta\varphi_{dB}\right) - c_{Na,0}}{\exp\left(\frac{F}{RT}\Delta\varphi_{dB}\right) - 1}$$

$$(19d)\quad (J_{K,dB})_{ss} = -\frac{n_d \tau_{m,d} D_{0,K}}{L_d} \frac{F}{RT} \Delta\varphi_{dB} \frac{c_{K,B} \exp\left(\frac{F}{RT}\Delta\varphi_{dB}\right) - c_{K,0}}{\exp\left(\frac{F}{RT}\Delta\varphi_{dB}\right) - 1}$$

where $\Delta\varphi_{dT}$ and $\Delta\varphi_{dB}$ are the liquid junction potentials across the top and bottom porous stones, respectively (Revil 1999):

$$(20a)\quad \Delta\varphi_{dT} = \frac{RT}{F} \cdot \ln\left[\frac{D_{0,Na} c_{Na,T} + D_{0,K} c_{K,T} + D_{0,Cl}(c_{Na,L} + c_{K,L})}{D_{0,Na} c_{Na,L} + D_{0,K} c_{K,L} + D_{0,Cl}(c_{Na,T} + c_{K,T})}\right]$$

$$(20b)\quad \Delta\varphi_{dB} = \frac{RT}{F} \cdot \ln\left[\frac{D_{0,Na} c_{Na,0} + D_{0,K} c_{K,0} + D_{0,Cl}(c_{Na,B} + c_{K,B})}{D_{0,Na} c_{Na,B} + D_{0,K} c_{K,B} + D_{0,Cl}(c_{Na,0} + c_{K,0})}\right]$$

Equations 19 and 20 hold true for perfectly flushing boundary conditions, i.e., when the imposed circulation rate is sufficiently fast for the average steady-state ionic concentrations at the upper and lower boundaries of the osmotic cell to be approximately equal to the values of the solutions used to replenish the flow-pump actuators. Such condition was judged to be satisfied for the multi-stage membrane test conducted in this study, since migration of ions through the bentonite specimen only caused a limited variation in the ionic concentrations of the solutions injected into and withdrawn from both boundaries of the osmotic cell (Table 2):

Fig. 8. Steady-state hydraulic head difference across the bentonite specimen, $(\Delta h)_{ss}$, as measured during the multi-stage membrane test (open symbols), and theoretical interpretation based on $\bar{c}'_{sk,0} = 180$ mM and $\tau_{m,b} = 0.22$ (continuous line). The chemico-osmotic and electro-osmotic contributions to the measured $(\Delta h)_{ss}$ are highlighted with short-dashed and long-dashed lines, respectively.

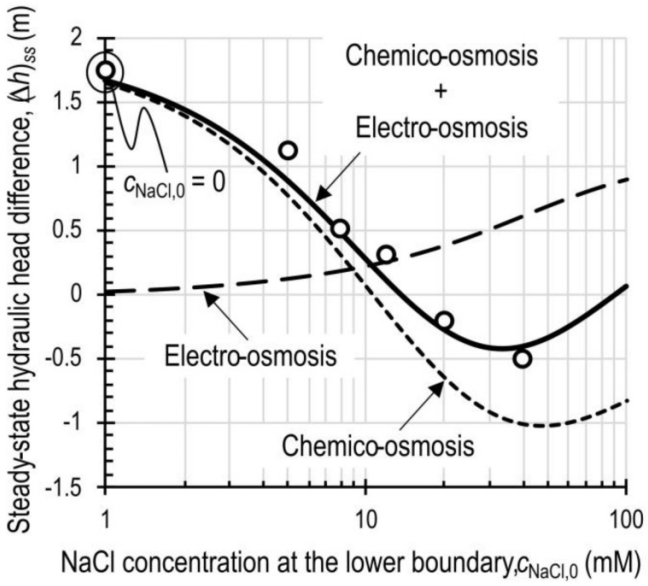

$$(21a)\quad c_{Na,L} = c_{NaCl,L}$$

$$(21b)\quad c_{K,L} = c_{KCl,L}$$

$$(21c)\quad c_{Na,0} = c_{NaCl,0}$$

$$(21d)\quad c_{K,0} = c_{KCl,0}$$

As a result of the hypothesis of perfectly flushing boundary conditions, any potential source of error that affected the measured ionic concentrations in the circulation outflows, as pointed out for the last testing stage, did not influence the calibration of the $\bar{c}'_{sk,0}$ and $\tau_{m,b}$ parameters and, ultimately, the assessment of the global reflection coefficient. $\bar{c}'_{sk,0}$ and $\tau_{m,b}$ were determined by fitting the experimental $(\Delta h)_{ss}$ values, which are listed in Table 2, to the theoretically predicted $(\Delta h)_{ss}$, using the mechanistic model developed by Guarena et al. (2022) and the calculation scheme outlined above to account for the effect of diffusion through the porous stones.

A high value of the coefficient of determination ($R^2 = 0.960$) was observed in correspondence to $\bar{c}'_{sk,0} = 180$ mM and $\tau_{m,b} = 0.22$, which allowed the membrane test results to be

Fig. 9. Ionic concentration profiles in the pore solution calculated for the third stage of the membrane test: (*a*) sodium (Na^+) ions; (*b*) potassium (K^+) ions; (*c*) chloride (Cl^-) ions.

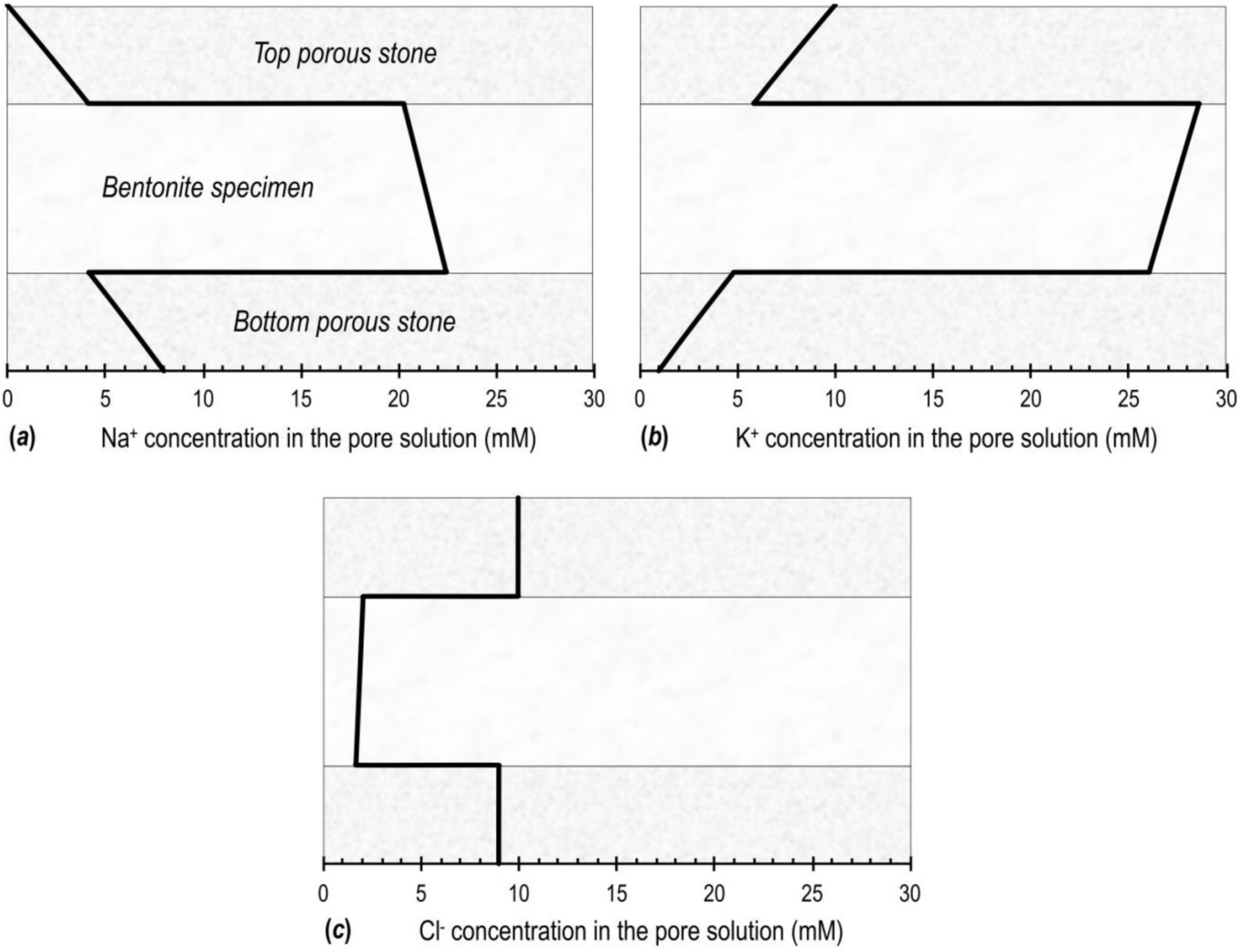

accurately interpreted. The obtained $\tau_{m,b}$ was consistent with the values that had been estimated by Dominijanni et al. (2018) (matrix tortuosity factor ranging from 0.187 to 0.203) for the same Indian sodium bentonite, as expected considering the similar porosities of the tested specimens (Guarena et al. 2024), whereas Dominijanni et al. (2018) reported a $\bar{c}'_{sk,0}$ value of 110 mM, which was considerably lower than the one obtained in the present study. This latter evidence suggests that working the bentonite with a spatula at a water content close to the liquid limit, prior to consolidation of the specimen and initiation of the membrane test, was effective in promoting dispersion of the soil fabric, which in turn resulted in a greater influence of the surface electrical charge on the coupled transport of water and ions.

The theoretical model developed by Guarena et al. (2022) is suitable for appreciating the different mechanisms that contributed to the build-up of the measured hydraulic head difference under null-volumetric-liquid-flux conditions. As illustrated in Fig. 8, the presence of a single salt (i.e., KCl), which dissociated into cations and anions with similar diffusivities, was associated with the predominant contribution of chemico-osmosis during the first testing stage, as the diffusion potential that was necessary to enforce the electric current density to be null was negligible. However, the presence of NaCl in the solution circulating through the lower boundary caused Na^+ ions to diffuse upwards from the bottom to the top porous stone during the subsequent testing stages, i.e., in the opposite direction to that of K^+ ions, with the system approaching a condition of pure counterdiffusion due to the low permeability of the bentonite specimen to Cl^- ions (Shackelford and Daniel 1991). This counterdiffusion of the cationic species in the absence of any significant diffusive flux of the anionic species is further enlightened in Fig. 9, which reports the concentration profiles of Na^+, K^+, and Cl^- ions in the pore solution calculated via the constant-field theory for the third testing stage ($c_{NaCl,0} = 8$ mM). If any other driving force had not been superimposed onto the ionic concentration gradients, a surplus of positive and negative electric charge would have accumulated at the lower and upper boundaries, respectively, as a result of purely diffusive transport. A negative diffusion potential, with the cathode corresponding to the top specimen boundary and the

Table 6. Results of the calculation of the reflection coefficient, ω_g, and diffusion potential, $\Delta\bar{\varphi}_b$, for the multi-stage membrane test conducted on the natural sodium bentonite.

			$\Delta\bar{\varphi}_b$(mV)		
$\Pi_L - \Pi_0$(kPa)	$\Pi_T - \Pi_B$(kPa)	ω_g(−)	Approximate solution	Exact solution	Error on $\Delta\bar{\varphi}_b$ (%)
43.87	24.49	0.694	0.021377	0.021381	0.0194
19.50	11.20	0.982	− 0.263890	− 0.263913	0.0088
4.87	4.81	1.040	− 0.396956	− 0.396964	0.0021
− 14.62	− 2.43	− 1.234	− 0.554123	− 0.554126	0.0005
− 53.62	− 14.19	0.141	− 0.826486	− 0.826748	0.0317
− 151.11	− 37.31	0.134	− 1.325133	− 1.328561	0.2580

Note: $\Pi_L - \Pi_0$, osmotic pressure difference between the boundaries of the osmotic cell; $\Pi_T - \Pi_B$, osmotic pressure difference between the boundaries of the bentonite specimen.

Fig. 10. Global reflection coefficient, ω_g, obtained from the multi-stage membrane test (open symbols), and theoretical interpretation based on $\bar{c}'_{sk,0} = 180$ mM and $\tau_{m,b} = 0.22$ (continuous line). The chemico-osmotic, Ω_c, and electro-osmotic contributions, Ω_e, to ω_g are highlighted with short-dashed and long-dashed lines, respectively.

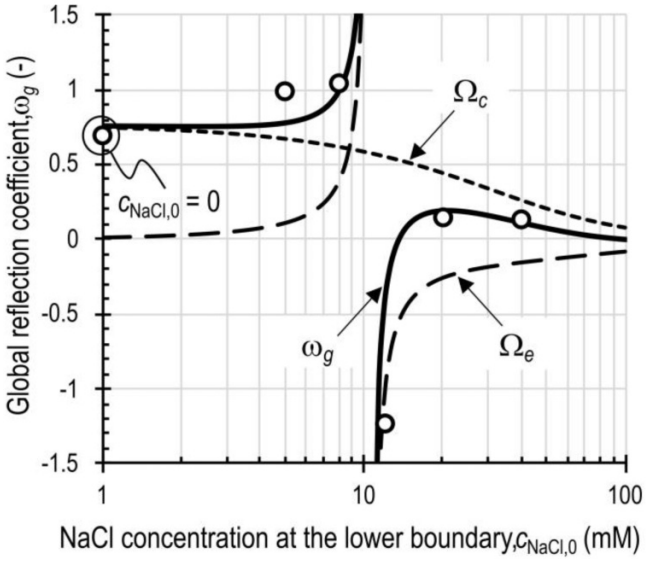

anode to the bottom specimen boundary, was thus generated to "speed up" the slower Na^+ ions and "slow down" the faster K^+ ions, so that a charge imbalance was prevented from occurring. Such electrically driven migration of cations towards the cathode was responsible for a net momentum transfer to the water molecules in the direction of more negative potential and, given the $q = 0$ condition, for the build-up of an electro-osmotic contribution to the measured hydraulic head difference, the magnitude of which was observed to increase upon an increase in $c_{NaCl,0}$. Unlike the chemico-osmotic contribution, which changed sign from positive to negative in correspondence to a null osmotic pressure difference across the specimen ($\Delta\Pi = 0$ at $c_{NaCl,0} = 10.58$ mM), the electro-osmotic contribution was always positive in sign and caused water movement in the same direction as that of chemico-osmosis during the second and third testing stages, i.e., when the solution circulating at the lower boundary corresponded to the hypotonic solution, and in the opposite direction to that of chemico-osmosis during the fourth, fifth, and sixth testing stages, i.e., when the solution circulating at the lower boundary corresponded to the hypertonic solution.

The imposed osmotic pressure difference between the boundaries of the osmotic cell, Π_L—Π_0, and the calculated osmotic pressure difference of the bulk solution between the boundaries of the bentonite specimen, Π_T—Π_B, the latter of which is simply denoted as $\Delta\Pi$ in the present study, are reported in Table 6 to stress the importance of accounting for diffusion through the porous stones when interpreting membrane test results. Indeed, diffusion through the porous stones caused a drop in Π_T—Π_B that ranged from less than 5% to more than 80% of Π_L—Π_0, thereby showing that ignoring the actual configuration of the three-layered system would have resulted in an incorrect assessment of the ionic concentrations at the specimen boundaries.

Once $\bar{c}'_{sk,0}$ and $\tau_{m,b}$ had been determined for the tested bentonite and $\Delta\Pi$ had been calculated for all the testing stages, the global reflection coefficient was obtained from the measured $(\Delta h)_{ss}$ according to eq. 8 (Table 6). The physical interpretation of the experimental values of ω_g, as illustrated in Fig. 10, shows that the occurrence of diffusion induced electro-osmosis during the second and third testing stages caused the global reflection coefficient to increase, relative to the (hypothetical) case of pure chemico-osmosis, which would have been observed if all the ionic species had diffused at the same rate in the pore solution. In particular, the extent of the electro-osmotic contribution at $c_{NaCl,0} = 8$ mM was such that ω_g resulted to be greater than unity ($\omega_g = 1.040$), which is the first and, at the time of writing, the only experimental evidence of positive anomalous osmosis in clay soils. On the other hand, the occurrence of diffusion induced electro-osmosis during the fourth, fifth, and sixth testing stages caused the global reflection coefficient to decrease, relative to the case of pure chemico-osmosis, and resulted in a value of ω_g at $c_{NaCl,0} = 12$ mM that was far lower than zero ($\omega_g = -1.234$), which is a manifestation of negative anomalous osmosis.

The calculation of the diffusion potential, which allowed the membrane test results to be theoretically interpreted, was based on the constant-field assumption. Although this approach accounts for the effect of nonlinearity in the ionic concentration profiles, an error was introduced by the

Fig. 11. Steady-state ionic molar fluxes, $(J_i)_{ss}$, as measured during the multi-stage membrane test (open symbols), and theoretical interpretation based on $\bar{c}'_{sk,0} = 180$ mM and $\tau_{m,b} = 0.22$ (continuous line): (*a*) Na^+ molar flux; (*b*) K^+ molar flux. $c_{NaCl,0}$, NaCl concentration of the solution injected into the lower boundary.

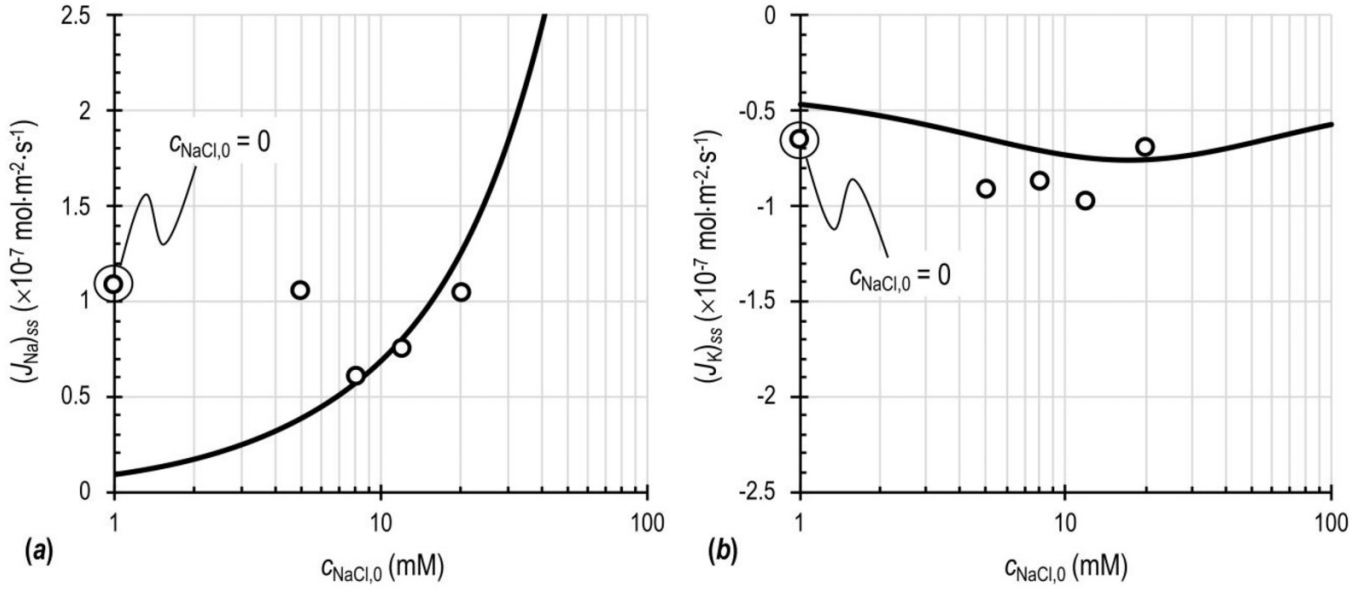

hypothesis of linearity in the electric potential profile, and this led to an approximate evaluation of $\Delta\bar{\varphi}_b$. With a view to assessing the magnitude of such error for the boundary conditions of the performed membrane test, the closed-form analytical solution derived by Guarena et al. (2022) was used to obtain an exact evaluation of $\Delta\bar{\varphi}_b$, which is reported in Table 6. Because of the high nonlinearity of the solving equations, the exact solution of $\Delta\bar{\varphi}_b$ derived by Guarena et al. (2022) could not be readily implemented within an automatic calculation algorithm to satisfy the condition of continuity in the ionic molar fluxes through the three-layered system, and therefore it was only used for the ionic concentrations that had previously been calculated at the specimen boundaries according to the constant-field theory. Albeit not rigorous, as the boundary ionic concentrations depend on the diffusion potential, the error on $\Delta\bar{\varphi}_b$ associated with the use of eq. 16 instead of the exact solution proposed by Guarena et al. (2022) could be quantified and was shown to always be lower than 3‰, thus suggesting that the constant-field theory closely approximates the actual distribution of the electric potential for the testing conditions considered herein.

Finally, the steady-state molar fluxes of Na^+ and K^+ ions, as measured for each testing stage and reported in Table 4, were compared with the theoretical predictions based on the values of $\bar{c}'_{sk,0}$ and $\tau_{m,b}$ previously calibrated with a view to interpreting the measured hydraulic head difference. Apart from the data pertaining to the early stages of the membrane test, which were affected by the presence of residual soluble NaCl in the bentonite pores, the fairly good agreement that can be observed in Fig. 11 further supports the conclusions that have been drawn about the role of diffusion induced electro-osmosis as the mechanism that is responsible for the observed osmotic anomalies.

Conclusions

A multi-stage membrane test was carried out on a natural sodium bentonite, which is used for the industrial production of a needle-punched geosynthetic clay liner, to measure its global reflection coefficient, ω_g, in equilibrium with aqueous solutions of mixed electrolytes. The concentrations of potassium chloride (KCl) of the solutions circulating through the upper and lower boundaries of the osmotic cell were kept constant and equal to 10 and 1 mM, respectively, while the concentration of sodium chloride (NaCl) of the solution circulating through the lower boundary was varied stepwise in the 0 to 40 mM range. The theoretical interpretation of the obtained test results demonstrated that the dominant contribution to the measured ω_g was the chemico-osmotic one when the testing solutions only comprised KCl, whereas the addition of NaCl to the solution circulating through the lower boundary was correlated with the enhanced influence of an electro-osmotic contribution, which was referred to as diffusion induced electro-osmosis and was caused by the different diffusivities of Na^+ and K^+ ions. Thus, the build-up of diffusion induced electro-osmosis was recognised as being the mechanism responsible for the occurrence of positive anomalous osmosis driving water in the direction of increasing osmotic pressure, with ω_g values as high as 1.040, and negative anomalous osmosis driving water in the direction of decreasing osmotic pressure, with ω_g values as low as –1.234.

As real contaminated liquids rarely consist of aqueous solutions of a single electrolyte, the occurrence of these osmotic anomalies in engineered bentonite-based barriers may be the norm rather than the exception for most chemical containment applications. In terms of the advective component of contaminant transport, positive anomalous osmosis

reflects a better containment performance than perfect or ideal semipermeable porous media ($\omega_g = 1$), whereas negative anomalous osmosis reflects a worse containment performance than non-semipermeable porous media ($\omega_g = 0$), so that, in the latter case, the classical (uncoupled) advective-diffusive transport theory does not necessarily yield a conservative assessment of the contaminant transport rate through such barriers.

Acknowledgements

The authors would like to thank Eni Rewind S.p.A. (Milan, Italy) for their financial support of this study and Roberto Maniscalco (former technician, Polytechnic University of Turin, Italy) for his cooperation in the development of the laboratory apparatus.

Article information

History dates

Received: 5 March 2024
Accepted: 24 July 2024
Accepted manuscript online: 29 July 2024
Version of record online: 15 October 2024

Copyright

Data availability

Data generated or analysed during this study are available from the corresponding author upon reasonable request.

Author information

Author ORCIDs

Nicolò Guarena https://orcid.org/0000-0001-5576-2078
Andrea Dominijanni https://orcid.org/0000-0002-0254-6002
Mario Manassero https://orcid.org/0000-0001-7621-5022

Author contributions

Conceptualization: NG, AD
Data curation: NG
Formal analysis: NG
Funding acquisition: NG, AD, MM
Investigation: NG
Methodology: NG, AD
Project administration: NG, AD, MM
Resources: NG
Supervision: AD, MM
Validation: NG
Visualization: NG
Writing – original draft: NG
Writing – review & editing: NG, AD

Competing interests

The authors declare that they have no known competing financial interests or personal relationships that could have appeared to influence the work reported in this paper.

References

Appelo, C.A.J., and Wersin, P. 2007. Multicomponent diffusion modeling in clay systems with application to the diffusion of tritium, iodide, and sodium in Opalinus Clay. Environmental Science & Technology, **41**(14): 5002–5007. doi:10.1021/es0629256.

Barbour, S.L., Lim, P.C., and Fredlund, D.G. 1996. A new technique for diffusion testing of unsaturated soil. Geotechnical Testing Journal, **19**(3): 247–258. doi:10.1520/GTJ10350J.

Bohnhoff, G.L., and Shackelford, C.D. 2013. Improving membrane performance via bentonite polymer nanocomposite. Applied Clay Science, **86**: 83–98. doi:10.1016/j.clay.2013.09.017.

Bohnhoff, G.L., and Shackelford, C.D. 2015. Salt diffusion through a bentonite-polymer composite. Clays and Clay Minerals, **63**(3): 145–162. doi:10.1346/CCMN.2015.0630301.

Bohnhoff, G.L., Shackelford, C.D., and Sample-Lord, K.M. 2014. Calcium-resistant membrane behavior of polymerized bentonite. Journal of Geotechnical and Geoenvironmental Engineering, **140**(3): 04013029. doi:10.1061/(ASCE)GT.1943-5606.0001042.

Di Emidio, G., Mazzieri, F., Verastegui-Flores, R.D., Van Impe, W., and Bezuijen, A. 2015. Polymer-treated bentonite clay for chemical-resistant geosynthetic clay liners. Geosynthetics International, **22**(1): 125–137. doi:10.1680/gein.14.00036.

Dominijanni, A., and Manassero, M. 2012*a*. Modelling the swelling and osmotic properties of clay soils. Part I: the phenomenological approach. International Journal of Engineering Science, **51**: 32–50. doi:10.1016/j.ijengsci.2011.11.003.

Dominijanni, A., and Manassero, M. 2012*b*. Modelling the swelling and osmotic properties of clay soils. Part II: the physical approach. International Journal of Engineering Science, **51**: 51–73. doi:10.1016/j.ijengsci.2011.11.001.

Dominijanni, A., Manassero, M., and Puma, S. 2013. Coupled chemical-hydraulic-mechanical behaviour of bentonites. Géotechnique, **63**(3): 191–205. doi:10.1680/geot.SIP13.P.010.

Dominijanni, A., Guarena, N., and Manassero, M. 2018. Laboratory assessment of semipermeable properties of a natural sodium bentonite. Canadian Geotechnical Journal, **55**(11): 1611–1631. doi:10.1139/cgj-2017-0599.

Dominijanni, A., Guarena, N., and Manassero, M. 2019*a*. Phenomenological analysis and physical interpretation of the reflection coefficient of clays. *In* Proceedings of the 8th International Congress on Environmental Geotechnics, Hangzhou, China, 28 October - 1 November 2018. *Edited by* L. Zhan, Y. Chen and A. Bouazza. Springer, Singapore, **Vol. 3**, pp. 156–163. doi:10.1007/978-981-13-2227-3_19.

Dominijanni, A., Fratalocchi, E., Guarena, N., Manassero, M., and Mazzieri, F. 2019*b*. Critical issues in the determination of the bentonite cation exchange capacity. Géotechnique Letters, **9**(3): 205–210. doi:10.1680/jgele.18.00229.

Elrick, D.E., Smiles, D.E., Baumgartner, N., and Groenevelt, P.H. 1976. Coupling phenomena in saturated homo-ionic montmorillonite: I. Experimental. Soil Science Society of America Journal, **40**(4): 490–491. doi:10.2136/sssaj1976.03615995004000040014x.

Evans, J.C., Shackelford, C.D., Yeo, S.S., and Henning, J. 2008. Membrane behavior of soil-bentonite slurry-trench cutoff walls. Soil and Sediment Contamination: Soil and Sediment Contamination: An International Journal, **17**(4): 316–322. doi:10.1080/15320380802143880.

Fu, X.L., Zhang, R., Reddy, K.R., Li, Y.C., Yang, Y.L., and Du, Y.J. 2021. Membrane behavior and diffusion properties of sand/SHMP-amended bentonite vertical cutoff wall backfill exposed to lead contamination. Engineering Geology, **284**: 106037. doi:10.1016/j.enggeo.2021.106037.

Glaus, M.A., Rossé, R., Van Loon, L.R., and Yaroshchuk, A.E. 2008. Tracer diffusion in sintered stainless steel filters: measurement of effective diffusion coefficients and implications for diffusion studies with compacted clays. Clays and Clay Minerals, **56**(6): 677–685. doi:10.1346/CCMN.2008.0560608.

Goldman, D.E. 1943. Potential, impedance, and rectification in membranes. Journal of General Physiology, **27**(1): 37–60. doi:10.1085/jgp.27.1.37.

Guarena, N., Dominijanni, A., and Manassero, M. 2020. From the design of bottom landfill liner systems to the impact assessment of contaminants on underlying aquifers. Innovative Infrastructure Solutions, **5**(1): 2. doi:10.1007/s41062-019-0251-y.

Guarena, N., Dominijanni, A., and Manassero, M. 2022. The role of diffusion induced electro-osmosis in the coupling between hydraulic and ionic fluxes through semipermeable clay soils. Soils and Foundations, **62**(4): 101177. doi:10.1016/j.sandf.2022.101177.

Guarena, N., Dominijanni, A., and Manassero, M. 2024. Pore-scale mechanisms underlying the behavior of enhanced bentonites exposed to aggressive inorganic solutions. Applied Clay Science, **251**: 107318. doi:10.1016/j.clay.2024.107318.

Guyonnet, D., Gaucher, E., Gaboriau, H., Pons, C.H., Clinard, C., Norotte, V., and Didier, G. 2005. Geosynthetic clay liner interaction with leachate: correlation between permeability, microstructure, and surface chemistry. Journal of Geotechnical and Geoenvironmental Engineering, **131**(6): 740–749. doi:10.1061/(ASCE)1090-0241(2005)131:6(740).

Hahn, O., and Woermann, D. 1996. Osmotic properties of a phenolsulfonic acid formaldehyde cation exchange membrane in contact with mixed aqueous electrolyte solutions. Journal of Membrane Science, **117**(1-2): 197–206. doi:10.1016/0376-7388(96)00053-1.

Henning, J., Evans, J.C., and Shackelford, C.D. 2006. Membrane behavior of two backfills from field-constructed soil-bentonite cutoff walls. Journal of Geotechnical and Geoenvironmental Engineering, **132**(10): 1243–1249. doi:10.1061/(ASCE)1090-0241(2006)132:10(1243).

Jougnot, D., Revil, A., and Leroy, P. 2009. Diffusion of ionic tracers in the Callovo-Oxfordian clay-rock using the Donnan equilibrium model and the formation factor. Geochimica et Cosmochimica Acta, **73**(10): 2712–2726. doi:10.1016/j.gca.2009.01.035.

Kang, J.B., and Shackelford, C.D. 2010. Membrane behavior of compacted clay liners. Journal of Geotechnical and Geoenvironmental Engineering, **136**(10): 1368–1382. doi:10.1061/(ASCE)GT.1943-5606.0000358.

Kang, J.B., and Shackelford, C.D. 2011. Consolidation enhanced membrane behavior of a geosynthetic clay liner. Geotextiles and Geomembranes, **29**(6): 544–556. doi:10.1016/j.geotexmem.2011.07.002.

Keijzer, Th.J.S., Kleingeld, P.J., and Loch, J.P.G. 1999. Chemical osmosis in compacted clayey material and the prediction of water transport. Engineering Geology, **53**(2): 151–159. doi:10.1016/S0013-7952(99)00028-9.

Kemper, W.D., and Quirk, J.P. 1972. Ion mobilities and electric charge of external clay surfaces inferred from potential differences and osmotic flow. Soil Science Society of America Journal, **36**(3): 426–433. doi:10.2136/sssaj1972.03615995003600030019x.

Malusis, M.A., and Daniyarov, A.S. 2016. Membrane efficiency and diffusive tortuosity of a dense prehydrated geosynthetic clay liner. Geotextiles and Geomembranes, **44**(5): 719–730. doi:10.1016/j.geotexmem.2016.05.006.

Malusis, M.A., and Shackelford, C.D. 2002a. Theory for reactive solute transport through clay membrane barriers. Journal of Contaminant Hydrology, **59**(3-4): 291–316. doi:10.1016/S0169-7722(02)00041-4.

Malusis, M.A., and Shackelford, C.D. 2002b. Chemico-osmotic efficiency of a geosynthetic clay liner. Journal of Geotechnical and Geoenvironmental Engineering, **128**(2): 97–106. doi:10.1061/(ASCE)1090-0241(2002)128:2(97).

Malusis, M.A., and Shackelford, C.D. 2002c. Coupling effects during steady-state solute diffusion through a semipermeable clay membrane. Environmental Science & Technology, **36**(6): 1312–1319. doi:10.1021/es011130q.

Malusis, M.A., Shackelford, C.D., and Olsen, H.W. 2001. A laboratory apparatus to measure chemico-osmotic efficiency coefficients for clay soils. Geotechnical Testing Journal, **24**(3): 229–242. doi:10.1520/GTJ11343J.

Malusis, M.A., Shackelford, C.D., and Olsen, H.W. 2003. Flow and transport through clay membrane barriers. Engineering Geology, **70**(3-4): 235–248. doi:10.1016/S0013-7952(03)00092-9.

Malusis, M.A., Shackelford, C.D., and Maneval, J.E. 2012. Critical review of coupled flux formulations for clay membranes based on nonequilibrium thermodynamics. Journal of Contaminant Hydrology, **138-139**: 40–59. doi:10.1016/j.jconhyd.2012.06.003.

Malusis, M.A., Kang, J.B., and Shackelford, C.D. 2015. Restricted salt diffusion in a geosynthetic clay liner. Environmental Geotechnics, **2**(2): 68–77. doi:10.1680/envgeo.13.00080.

Malusis, M.A., Scalia, J., Norris, A.S., and Shackelford, C.D. 2020. Effect of chemico-osmosis on solute transport in clay barriers. Environmental Geotechnics, **7**(7): 447–456. doi:10.1680/jenge.17.00109.

Malusis, M.A., Dominijanni, A., Scalia, J., Guarena, N., Sample-Lord, K.M., Bohnhoff, G.L., et al. 2021. Assessing the influence of chemico-osmosis on solute transport in bentonite membranes based on combined phenomenological and physical modeling. Japanese Geotechnical Society Special Publication, **9**(2): 37–44. doi:10.3208/jgssp.v09.cpeg023.

Manassero, M. 2020. Second ISSMGE R. Kerry Rowe Lecture: on the intrinsic, state, and fabric parameters of active clays for contaminant control. Canadian Geotechnical Journal, **57**(3): 311–336. doi:10.1139/cgj-2019-0033.

Manassero, M., and Dominijanni, A. 2003. Modelling the osmosis effect on solute migration through porous media. Géotechnique, **53**(5): 481–492. doi:10.1680/geot.2003.53.5.481.

Manassero, M., and Shackelford, C.D. 1994. The role of diffusion in contaminant migration through soil barriers. Rivista Italiana di Geotecnica, **28**(1): 5–31.

Manassero, M., Dominijanni, A., and Guarena, N. 2018. Modelling hydro-chemo-mechanical behaviour of active clays through the fabric boundary surface. *In* Proceedings of China-Europe Conference on Geotechnical Engineering, Vienna, Austria, 13-16 August 2018. *Edited by* W. Wu and H.S. Yu. Springer Series in Geomechanics and Geoengineering, Cham, Switzerland, **Vol. 2**, pp. 1618–1626. doi:10.1007/978-3-319-97115-5_157.

Marine, I.W., and Fritz, S.J. 1981. Osmotic model to explain anomalous hydraulic heads. Water Resources Research, **17**(1): 73–82. doi:10.1029/WR017i001p00073.

Mazzieri, F., Di Emidio, G., and Van Impe, P.O. 2010. Diffusion of calcium chloride in a modified bentonite: impact on osmotic efficiency and hydraulic conductivity. Clays and Clay Minerals, **58**(3): 351–363. doi:10.1346/CCMN.2010.0580306.

Meier, A.J., and Shackelford, C.D. 2017. Membrane behavior of compacted sand–bentonite mixture. Canadian Geotechnical Journal, **54**(9): 1284–1299. doi:10.1139/cgj-2016-0708.

Mitchell, J.K., and Soga, K. 2005. Fundamentals of soil behavior. 3rd ed. John Wiley & Sons, New York, USA.

Musso, G., Cosentini, R.M., Dominijanni, A., Guarena, N., and Manassero, M. 2017. Laboratory characterization of the chemo-hydro-mechanical behaviour of chemically sensitive clays. Rivista Italiana di Geotecnica, **51**(3): 22–47. doi:10.19199/2017.3.0557-1405.022.

Ni, H., Shen, S.Q., Fu, X.L., Wang, C.M., and Du, Y.J. 2022. Assessment of membrane and diffusion behavior of soil-bentonite slurry trench wall backfill consisted of sand and Xanthan gum amended bentonite. Journal of Cleaner Production, **365**: 132779. doi:10.1016/j.jclepro.2022.132779.

Olsen, H.W., Yearsley, E.N., and Nelson, K.R. 1989. Chemical causes of groundwater movement. *In* Groundwater Contamination. *Edited by* L.M. Abriola. Publication 185, IAHS, pp. 65–72.

Revil, A. 1999. Ionic diffusivity, electrical conductivity, membrane and thermoelectric potentials in colloids and granular porous media: a unified model. Journal of Colloid and Interface Science, **212**(2): 503–522. doi:10.1006/jcis.1998.6077.

Revil, A., and Leroy, P. 2004. Constitutive equations for ionic transport in porous shales. Journal of Geophysical Research: Solid Earth, **109**: B03208. doi:10.1029/2003JB002755.

Sample-Lord, K.M., and Shackelford, C.D. 2016. Dialysis method to control exchangeable sodium and remove excess salts from bentonite. Geotechnical Testing Journal, **39**(2): 206–216. doi:10.1520/GTJ20150065.

Sample-Lord, K.M., and Shackelford, C.D. 2018. Membrane behavior of unsaturated sodium bentonite. Journal of Geotechnical and Geoenvironmental Engineering, **144**(1): 04017102. doi:10.1061/(ASCE)GT.1943-5606.0001803.

Shackelford, C.D. 1991. Laboratory diffusion testing for waste disposal—a review. Journal of Contaminant Hydrology, **7**(3): 177–217. doi:10.1016/0169-7722(91)90028-Y.

Shackelford, C.D. 2013. Membrane behavior in engineered bentonite-based containment barriers: state of the art. *In* Proceedings of the International Symposium on Coupled Phenomena in Environmental Geotechnics, Torino, Italy, 1-3 July 2013. *Edited by* M. Manassero, A. Dominijanni, S. Foti and G. Musso. CRC Press/Balkema, Taylor & Francis Group, London, England, UK, pp. 45–60. doi:10.1201/b15004-7.

Shackelford, C.D., and Daniel, D.E. 1991. Diffusion in saturated soil: I. Background. Journal of Geotechnical Engineering, **117**(3): 467–484. doi:10.1061/(ASCE)0733-9410(1991)117:3(467).

Shackelford, C.D., and Lee, J.M. 2003. The destructive role of diffusion on clay membrane behavior. Clays and Clay Minerals, **51**(2): 186–196. doi:10.1346/CCMN.2003.0510209.

Shackelford, C.D., Meier, A.J., and Sample-Lord, K.M. 2016. Limiting membrane and diffusion behavior of a geosynthetic clay liner. Geotextiles and Geomembranes, **44**(5): 707–718. doi:10.1016/j.geotexmem.2016.05.009.

Shackelford, C.D., Lu, N., Malusis, M.A., and Sample-Lord, K.M. 2019. Research challenges involving coupled flows in geotechnical engineering. *In* Geotechnical Fundamentals for Addressing New World Challenges. *Edited by* N. Lu and J.K. Mitchell. Springer Series in Geomechanics and Geoengineering, Cham, Switzerland, pp. 237–274. doi:10.1007/978-3-030-06249-1_9.

Tang, Q., Katsumi, T., Inui, T., and Li, Z. 2014. Membrane behavior of bentonite-amended compacted clay. Soils and Foundations, **54**(3): 329–344. doi:10.1016/j.sandf.2014.04.019.

Tang, Q., Katsumi, T., Inui, T., and Li, Z. 2015. Influence of pH on the membrane behavior of bentonite amended Fukakusa clay. Separation and Purification Technology, **141**: 132–142. doi:10.1016/j.seppur.2014.11.035.

Tong, S., and Sample-Lord, K.M. 2022. Coupled solute transport through a polymer-enhanced bentonite. Soils and Foundations, **62**(6): 101235. doi:10.1016/j.sandf.2022.101235.

van't Hoff, J.H. 1887. The role of osmotic pressure in the analogy between solutions and gases. Zeitschrift für physikalische Chemie, **1**: 481–508.

Yaroshchuk, A.E., and Van Loon, L.R. 2008. Improved interpretation of in-diffusion measurements with confined swelling clays. Journal of Contaminant Hydrology, **97**(1-2): 67–74. doi:10.1016/j.jconhyd.2007.12.003.

Yaroshchuk, A.E., Röttger, H., and Woermann, D. 1993. Osmotic properties of a cation exchange membrane: reflection coefficients of a solute larger than 1 in a system with aqueous mixed electrolyte solutions. Berichte der Bunsengesellschaft für Physikalische Chemie, **97**(5): 676–679. doi:10.1002/BBPC.19930970506.

Yaroshchuk, A.E., Glaus, M.A., and Van Loon, L.R. 2008. Diffusion through confined media at variable concentrations in reservoirs. Journal of Membrane Science, **319**(1-2): 133–140. doi:10.1016/j.memsci.2008.03.027.

Yaroshchuk, A.E., Glaus, M.A., and Van Loon, L.R. 2009. Determination of diffusion and sorption parameters of thin confined clay layers by direct fitting of through-diffusion flux. Journal of Colloid and Interface Science, **337**(2): 508–512. doi:10.1016/j.jcis.2009.05.049.

Yeo, S.S., Shackelford, C.D., and Evans, J.C. 2005. Membrane behavior of model soil-bentonite backfill mixtures. Journal of Geotechnical and Geoenvironmental Engineering, **131**(4): 418–429. doi:10.1061/(ASCE)1090-0241(2005)131:4(418).